INTERNATIONAL JOURNAL FOR NUMERICAL METHODS IN FLUIDS
*Int. J. Numer. Meth. Fluids* 2005; **49**:1111–1146
Published online 3 August 2005 in Wiley InterScience (www.interscience.wiley.com). DOI: 10.1002/fld.1041

# A semi-Lagrangian level set method for incompressible Navier–Stokes equations with free surface

Leo Miguel González Gutiérrez[1,*,†] and Rodolfo Bermejo[2,‡]

[1] *Universidad Pontificia Comillas de Madrid, C/Alberto Aguilera 23, 28015 Madrid, Spain*
[2] *Departamento de Matemática Aplicada, Universidad Politécnica de Madrid, ETS de Ingenieros Industriales, José Guitiérrez Abascal, 2, 28006 Madrid, Spain*

## SUMMARY

In this paper, we formulate a level set method in the framework of finite elements-semi-Lagrangian methods to compute the solution of the incompressible Navier–Stokes equations with free surface. In our formulation, we use a quasi-monotone semi-Lagrangian scheme, which is both unconditionally stable and essentially non oscillatory, to compute the advective terms in the Navier–Stokes equations, the transport equation and the equation of the reinitialization stage for the level set function. The method we propose is quite robust and flexible with regard to the mesh and the geometry of the domain, as well as the magnitude of the Reynolds number. We illustrate the performance of the method in several examples, which range from a benchmark problem to test the volume conservation property of the method to the flow past a NACA0012 foil at high Reynolds number. Copyright © 2005 John Wiley & Sons, Ltd.

KEY WORDS: quasi-monotone semi-Lagrangian schemes; level set method; characteristics; finite elements; Navier–Stokes; free surface

## 1. INTRODUCTION

There are many flows in engineering applications with interfaces and free surfaces. As examples of such flows we can think of combustion problems, incompressible two-phase flows, flow around a body on the sea surface and so on. The mathematical formulation of these problems consists of the Navier–Stokes equations with different additional terms to

[*] Correspondence to: Leo Miguel González Gutiérrez, Universidad Pontificia Comillas de Madrid, C/Alberto Aguilera 23, 28015 Madrid, Spain.
[†] E-mail: lmgonzalez@dfc.icai.upco.es
[‡] E-mail: rbermejo@etsii.upm.es

Contract/grant sponsor: Comisión Interministerial de Ciencia y Tecnología de España; contract/grant number: CLI98-1076
Contract/grant sponsor: Ministerio de Ciencia y Tecnología de España; contract/grant number: REN2002-03726

*Received 30 April 2004*
*Revised 11 February 2005*
*Accepted 11 April 2005*

model the surface tension and the volume and reaction forces, if necessary, plus the equation describing the motion of the interfaces and the free surfaces. The presence of interfaces and/or the free surfaces as a part of the solution of the problem increases the degree of difficulty of the Navier–Stokes equations. Many researchers have devoted their efforts to devise '*ad hoc*' numerical methods to deal with the specific difficulties brought about by the motion of the interfaces and free surfaces, in particular, when they undergo severe deformations. There are two approaches frequently used in the numerical modelling community, namely, the front tracking technique and the front capturing technique. The former one gives the position of the interfaces by explicitly tracking their displacements, whereas the latter one computes such a position via a smooth function that satisfies an equation to be solved as part of the problem. Based on this idea, the level set method was introduced in Reference [1] to calculate the motion of interfaces. Since then, the level set methodology has been used in a large range of problems [2, 3]. Most of the numerical formulations of the level set are constructed on square uniform grids and use advection schemes of the ENO family.

In this paper, we shall apply the level set method to compute the solution of the incompressible Navier–Stokes equations with free surface as they are used in Marine Hydrodynamics to study the viscous flow around ships or submerged bodies at low depth. In these problems, it is important to calculate with good accuracy the position of the free surface because it has a strong influence on both, the type of flow developed around the body and the flow forces acting on it. Many of the codes developed for the past fifteen years to calculate the numerical solution of viscous flow around a body, in the presence of a free surface, are based on the MAC formulation [4] and use a tracking technique to follow the motion of a number of markers located on the free surface [5], such that the positions of these markers will determine the location of the free surface. Recently, however, there have appeared some papers, References [6, 7], in which the level set method is proposed as an interesting and competitive method to be used in the computation of flow around a submerged body in the presence of a free surface because with this method no remeshing is done during the calculation. The level set formulation of References [6–8] is based on the methods first proposed in Reference [9] to compute the solutions for incompressible two-phase flows. These papers construct the finite difference formulation of the Navier–Stokes equations in a square uniform grid and use a second-order ENO scheme to compute the solutions of both, the advection equation and the reinitialization of the level set function. Following the level set approach, we present in this paper a numerical method to calculate an approximate solution of the incompressible Navier–Stokes equations with free surface the main feature of which is the semi-Lagrangian scheme to calculate the level set function. A semi-Lagrangian approach has already been used by Strain, see, for instance, References [10, 11], to solve the level set equations; however, our semi-Lagrangian approach for the level set function equation and its reinitialization correction differs from Strain's one in some respects. The motivation to use a semi-Lagrangian scheme comes from the fact that the level set equation is an homogeneous transport equation and articles like [12–14] show that these schemes work well with this kind of equation. At this point of this introductory section we do not wish to go into the description of such details; however, we should mention the following differences: (i) We use a higher order quasi-monotone Lagrange interpolation procedure to compute the values of both the flow velocity and the level set function at the departure points of the trajectories. Since Lagrange interpolation is not restricted by the spatial dimensions of the problem nor by the type of mesh [15], our quasi-monotone interpolation is very general in the sense that it is suitable for any type of mesh without any additional effort. We should understand quasi-monotone interpolation as positive interpolation or, better perhaps, as a type of essentially non oscillatory interpolation because it can hold oscillations with amplitude $O(h^{p+1})$, where $h$ denotes the mesh size parameter and $p$ the degree of the polynomial interpolation. Moreover, our method to provide quasi-monotonicity is not specifically designed for Lagrange interpolation; on the contrary, it can be executed as well with Hermite interpolation, spline interpolation or even trigonometric interpolation. (ii) We do reinitialization (redistancing) of the level set function by using Sussman and Fatemi algorithm [16] in our semi-Lagrangian framework. The numerical solution of the Navier–Stokes equations is calculated as proposed by Allievi and Bermejo in Reference [12], using the quasi-monotone extension of the conventional semi-Lagrangian interpolation first introduced in Reference [14].

## 2. EQUATIONS OF MOTION

We wish to compute the approximate solution of the flow past a solid body, which is submerged in a water domain $D_1$ where one of the boundaries is a free surface. See Figure 1 for the geometrical setting of our model problem. The governing equations are the incompressible Navier–Stokes equations, which have to be supplemented with dynamic and kinematic boundary conditions on the free surface together with the conventional boundary conditions on solid and open boundaries. Following the formulation of Reference [9] we embed our fluid domain in a larger domain $D$ that contains two immiscible fluids, one is water (the water variables are denoted by subscript 1) and the other one is air (with its corresponding variables denoted by the subscript 2) of densities and viscosities $\rho_i$ and $\mu_i$ $(i=1,2)$, respectively, such that if $\overline{D}_i = D_i \cup \Gamma_i \cup \Gamma_0\, (i=1,2)$, $\Gamma_i \cup \Gamma_0$ being the boundary of $D_i$, and $\Gamma_0 = \overline{D}_1 \cap \overline{D}_2$, we define $D = \Gamma_0 \cup D_1 \cup D_2$ and $\partial D$ the boundary of $D$. Notice that $\Gamma_0$ represents the free surface of the water body. For numerical purposes, the air is considered to be an incompressible fluid. This is a reasonable assumption because in this problem the air velocity is much smaller than the

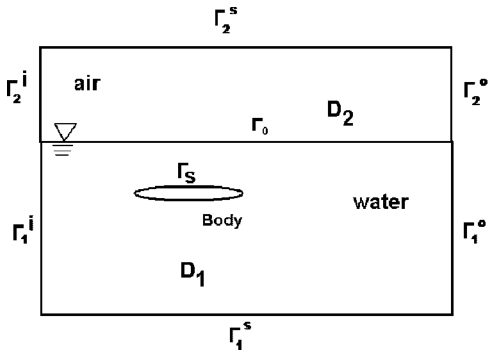

Figure 1. General geometry. $D_1$ and $D_2$ water and air domains, respectively, with boundaries: inflow, $\Gamma_1^{\mathrm{i}}$ and $\Gamma_2^{\mathrm{i}}$; outflow $\Gamma_1^{\mathrm{o}}$ and $\Gamma_2^{\mathrm{o}}$; solids $\Gamma_1^{\mathrm{s}}$ and $\Gamma_2^{\mathrm{s}}$; free boundary $\Gamma_0$. Solid body with boundary $\Gamma_{\mathrm{S}}$.

speed of sound. Thus, the governing equations are

$$\begin{aligned}\frac{\mathrm{D}\rho\mathbf{u}}{\mathrm{D}t}+\nabla p=\nabla\cdot\mu\nabla\mathbf{u}+\mathbf{F}+\sigma\kappa\mathbf{n}_{\Gamma_0}\delta_{\Gamma_0}(d)\quad\text{in } D\times(0,T)\\ \nabla\cdot\mathbf{u}=0\quad\text{in } D\times(0,T)\end{aligned}\tag{1}$$

where $\mathbf{u}$ is the velocity vector and $p$ is the pressure; $\mathbf{F}$ is the vector of body forces which include the gravity force, so that, we express the vector of body forces as $\mathbf{F}=\mathbf{f}(x,t)-\rho g\nabla z$, $z$ being the vertical coordinate; $\sigma$ represents the surface tension; $\kappa$ and $\mathbf{n}_{\Gamma_0}$ denote the mean curvature and the unit normal vector at the interface $\Gamma_0$; $\delta_{\Gamma_0}(d)$ is the Dirac delta function and $d$ is the normal distance to the interface. The material derivative of a physical variable $a$ is given by

$$\frac{\mathrm{D}a}{\mathrm{D}t}=\frac{\partial a}{\partial t}+\mathbf{u}\cdot\nabla a\tag{2}$$

and measures the variation of $a$ along the trajectories of the fluid particles. As initial conditions for (1) we shall have

$$\mathbf{u}(x,0)=\mathbf{u}_0(x)\quad\text{in } D\tag{3}$$

where $\mathbf{u}_0(x)$ is a prescribed velocity in the domain $D$. As boundary conditions, we consider the following:

(i) *Solid boundaries* ($\Gamma_1^{\mathrm{s}}$, $\Gamma_2^{\mathrm{s}}$ and $\Gamma_{\mathrm{S}}$):

$$\mathbf{u}=0\quad\forall t\tag{4}$$

(ii) *Outflow boundaries* ($\Gamma_1^{\mathrm{o}}$ and $\Gamma_2^{\mathrm{o}}$):

$$-p\mathbf{n}+\rho v\frac{\partial\mathbf{u}}{\partial\mathbf{n}}+\rho\mathbf{g}z\cdot\mathbf{n}=0\quad\forall t\tag{5}$$

where $\mathbf{n}$ denotes the unitary outward normal vector at the boundary, $\mathbf{g}$ is the gravity acceleration vector, $z$ is the vertical coordinate and $v=\frac{\mu}{\rho}$ is the dynamical viscosity.

(iii) *Inflow boundaries* ($\Gamma_1^{\mathrm{i}}$ and $\Gamma_2^{\mathrm{i}}$):

$$-\mathbf{n}\cdot\mathbf{u}=b(t)\tag{6}$$

where $b(t)$ is a prescribed normal velocity.

For immiscible fluids, densities satisfy the equation

$$\frac{\mathrm{D}\rho}{\mathrm{D}t}=0\quad\text{in } D\times(0,T)\tag{7}$$

## 3. LEVEL SET FORMULATION

Following the approach of Reference [9] we can consider the free surface $\Gamma_0$ as the zero level set of a function $\phi(x,t)$, termed level set function, and link the evolution of $\phi$ to the motion of the free surface via an initial value problem for $\phi$. Specifically, at any time $t \in [0,T]$ the free surface is defined as

$$\Gamma_0(t) = \{x \in D\colon \phi(x(t),t) = 0\} \tag{8}$$

then, since $\phi(x,t)$ is a level set function, i.e. $\phi(x,t) = C$, it follows that

$$\frac{\mathrm{D}\phi}{\mathrm{D}t} = \frac{\partial \phi}{\partial t} + \mathbf{u} \cdot \nabla \phi = 0 \tag{9}$$

with the initial condition

$$\phi(x,0) = \pm \min_{y \in \Gamma_0(0)} |x-y| \quad \forall x \in D \tag{10}$$

where $|x-y|$ denotes, unless otherwise stated, the Euclidean distance between the points $x$ and $y$ and $\mathbf{u} = \mathrm{d}x/\mathrm{d}t$ denotes the velocity of the fluid particles. This means that when $x(t) \in \Gamma_0(t)$ $\mathbf{u}$ represents the velocity of the points of the free surface. As level set function $\phi(x,t)$ we choose the signed normal distance to the free surface, i.e.

$$\phi(x,t) = \pm \min_{y \in \Gamma_0(t)} |x-y| \quad \forall x \in D \tag{11}$$

so that, for all $t$, we can characterize $\phi(x,t)$ by the following properties:

$$|\nabla \phi| = 1 \tag{12}$$

and

$$\phi(x,t) \begin{cases} >0 & \text{if } x \in D_1 \\ =0 & \text{if } x \in \Gamma(t) \\ <0 & \text{if } x \in D_2 \end{cases} \tag{13}$$

It is interesting to note that (9) moves the zero level set $\phi(x,t) = 0$ at the correct velocity, but $\phi(x,t)$ as solution of (9) will no longer remain a signed normal distance function, i.e. $|\nabla \phi| \neq 1$, so that, in order to make $\phi$ be a signed normal distance we shall use a reinitialization procedure that is described below.

By virtue of (7)–(13) we can express the densities $\rho_i$ and viscosities $\mu_i$ as functions of $\phi$ as follows:

$$\rho(\phi) = \rho_2 \left(1 + \left(\frac{\rho_1}{\rho_2} - 1\right) H(\phi)\right) \tag{14}$$

and

$$\mu(\phi) = \mu_2 \left(1 + \left(\frac{\mu_1}{\mu_2} - 1\right) H(\phi)\right) \tag{15}$$

where $H(\phi)$ is the Heaviside function given by

$$H(\phi) = \begin{cases} 0 & \text{if } \phi < 0 \\ (0,1) & \text{if } \phi = 0 \\ 1 & \text{if } \phi > 0 \end{cases} \tag{16}$$

Using the notation of (14) and (15), it is quite common to write (1) in non-dimensional form by introducing the dimensionless variables

$$x = Lx', \quad \mathbf{u} = U_0\mathbf{u}', \quad t = \left(\frac{L}{U_0}\right)t'$$

$$p = \rho_1 U_0^2 p', \quad \rho = \rho_1\rho', \quad \mu = \mu_1\mu', \quad \mathbf{f} = \frac{U_0^2}{L}\mathbf{f}'$$

where the superscript denotes dimensionless variables and $L$ and $U_0$ are length and velocity scales of reference, respectively. Thus, dropping the superscript by notational simplicity, we have that in $D \times (0, T]$

$$\begin{aligned} &\frac{\mathrm{D}\rho(\phi)\mathbf{u}}{\mathrm{D}t} + \nabla p = \frac{-1}{F_r^2}\nabla z + \left(\frac{1}{Re}\nabla\cdot(\rho(\phi)\upsilon(\phi)\nabla\mathbf{u}) + \frac{1}{We}\sigma\kappa(\phi)\delta(\phi)\nabla\phi\right) + \mathbf{f} \\ &\nabla\cdot\mathbf{u} = 0 \end{aligned} \tag{17}$$

where

$$\rho(\phi) = \frac{\rho_2}{\rho_1} + \left(1 - \frac{\rho_2}{\rho_1}\right)H(\phi), \quad \mu(\phi) = \frac{\mu_2}{\mu_1} + \left(1 - \frac{\mu_2}{\mu_1}\right)H(\phi) \tag{18}$$

the Reynolds number

$$Re = \frac{\rho_1 U_0 L}{\mu_1}$$

the Froude number

$$Fr = \frac{U_0^2}{gL}$$

and the Weber number

$$We = \frac{\rho_1 L U_0^2}{\sigma}$$

$We$ is very large for the class of marine hydrodynamic problems we intend to solve, so that, in the sequel we shall drop the surface tension terms from the equations.

### *3.1. Smoothing at the interface*

The sharp change that $\rho$ and $\mu$ experience at the interface $\Gamma_0(t)$ poses a serious problem for numerical computations. This problem causes the presence of wiggles in the numerical solution that may deteriorate the rate of convergence for the future time steps. One method to alleviate such problems is proposed in Reference [17] by assuming the existence of a transition region $[-\alpha, \alpha]$ where the free surface is embedded. The semi-thickness $\alpha$ is proportional to the mesh size $h$. Then, we replace $\rho(\phi)$, $\mu(\phi)$ and $H(\phi)$ by the smooth functions

$$\rho_\alpha(\phi)=\frac{\rho_2}{\rho_1}+\left(1-\frac{\rho_2}{\rho_1}\right)H_\alpha(\phi), \quad \mu_\alpha(\phi)=\frac{\mu_2}{\mu_1}+\left(1-\frac{\mu_2}{\mu_1}\right)H_\alpha(\phi) \tag{19}$$

and

$$H_\alpha(\phi)=\begin{cases} 0 & \text{if } \phi<-\alpha \\ \frac{1}{2}\left[1+\frac{\phi}{\alpha}+\frac{1}{\pi}\sin\left(\frac{\pi\phi}{\alpha}\right)\right] & \text{if } |\phi|\leqslant\alpha \\ 1 & \text{if } \phi>\alpha \end{cases} \tag{20}$$

respectively. Also, we define both a smooth delta function $\delta_\alpha(\phi)$ as the derivative with respect to $\phi$ of $H_\alpha(\phi)$, then

$$\delta_\alpha(\phi)=\begin{cases} \frac{1}{2\alpha}\left[1+\cos\left(\left(\frac{\pi\phi}{\alpha}\right)\right)\right] & \text{if } |\phi|\leqslant\alpha \\ 0 & \text{otherwise} \end{cases} \tag{21}$$

and the sign function as

$$\text{sign}_\alpha(\phi)=2H_\alpha(\phi)-1 \tag{22}$$

### 3.2. Reinitialization

As we have already mentioned, (9) moves the interface at the right velocity but its solution $\phi$ is not a signed normal distance function and may become irregular after a few time steps. To remedy these drawbacks, Sussman and Fatemi [16] and Sussman *et al.* [9, 17] propose a reinitialization procedure to restore such a character to $\phi$. This is achieved by solving, until the steady state is reached, the non linear hyperbolic problem

$$\begin{gathered} \frac{\partial d(x,t;\tau)}{\partial\tau}+\mathbf{w}\cdot\nabla d=\text{sign}(\phi(x,t)) \quad \text{in } D \\ d(x,t;0)=\phi(x,t) \quad \text{in } D \end{gathered} \tag{23}$$

where $\tau$ is a pseudo time variable, $\phi(x,t)$ is the solution of (9) and (10) at time $t$ and $\mathbf{w}$ plays the role of an advection velocity the expression of which is

$$\mathbf{w}=\text{sign}(\phi)\frac{\nabla d}{|\nabla d|} \tag{24}$$

Note that $\mathbf{w}$ points away from the zero level set with modulus equal to 1, so that the characteristics of (23) propagate away from the interface with speed one while maintaining fixed the position of the interface $\Gamma_0(\tau)$ . Sussman and Fatemi [16] calculate the solution of (23) by the method of characteristics for small times. This solution shows the interesting property that there is a time $\tau_{\text{steady}}$ such that for $\tau\geqslant\tau_{\text{steady}}$ the solution $d$ reaches the steady state $d_{\text{steady}}$

satisfying

$$\operatorname{sign}(\phi)(1-|\nabla d_{\text{steady}}|)=0 \quad \text{in } D$$

so that the new level set function $\phi(x,t)=d(x,t;\tau_{\text{steady}})$ is again a signed normal distance. On the other hand, by solving (23) does not change the position of the interface $\Gamma_0(t)$, thereby, the solution of (23) conserves the volume of the fluid domain bounded by $\Gamma_0(t)$ and $D_1$. Unfortunately, in the numerical solution this property does not, in general, hold; so that to enforce the conservation of volume on the numerical solution, Sussman and Fatemi [16] use the Lagrange multiplier technique modifying (23) as

$$\begin{aligned}\frac{\partial d(t,x;\tau)}{\partial\tau}+\mathbf{w}\cdot\nabla d-\operatorname{sign}(\phi(x,t))-\lambda(\tau)f(d)=0 \quad \text{in } D\\ d(x,t;0)=\phi(x,t) \quad \text{in } D\end{aligned} \tag{25}$$

where $\lambda$ is the Lagrange multiplier which is determined by taking into account that for any fixed volume $W$

$$\frac{\mathrm{d}}{\mathrm{d}\tau}\int_W H(d)\,\mathrm{d}x=0$$

implies, by virtue of (25), that

$$\begin{aligned}\frac{\mathrm{d}}{\mathrm{d}\tau}\int_W H(d)\,\mathrm{d}x=\int_W H'(d)\frac{\partial d}{\partial\tau}\,\mathrm{d}x=-\int_W H'(d)(\mathbf{w}\cdot\nabla d\\ -\operatorname{sign}(\phi(x,t))-\lambda(\tau)f(d))\,\mathrm{d}x=0\end{aligned}$$

Hence

$$\lambda=\frac{\int_W H'(d)(\mathbf{w}\cdot\nabla d-\operatorname{sign}(\phi(x,t)))\,\mathrm{d}x}{\int_W H'(d)f(d)\,\mathrm{d}x} \tag{26}$$

As for $f(d)$, Sussman and Fatemi [16] propose

$$f(d)=H'(d)|\nabla d| \tag{27}$$

this means that the correction is applied at the transition band only.

## 4. NUMERICAL FORMULATION

We introduce in this section the numerical method to solve the Navier–Stokes problem (1)–(6), the transport problem for the level set function (9) and (10) and the reinitialization problem (23). The intrinsic numerical difficulties that these problems pose are the following: (i) In the Navier–Stokes equations, the non linearity of the material derivative $\mathrm{D}\mathbf{u}/\mathrm{D}t$ and the constraint $\nabla\cdot\mathbf{u}=0$. (ii) In the level set function equation we would like to obtain a numerical approximation to $\phi$ free of oscillations; and (iii) the hyperbolic and non linear nature of Equation (23). We can also have other difficulties associated with the geometry of the domain and the need to have a finer mesh in selected areas of the domain such as the band that contains the free surface, boundary layers, regions of low regularity and so on. Several researchers [9, 16, 17] have proposed efficient methods to deal with the intrinsic difficulties (i)–(iii); for instance, they propose a projection scheme for the Navier–Stokes equations and upwind schemes of the ENO family to solve the level set and reinitialization equations in the framework of finite differences for space discretization of the differential operators. Others authors as Barth and Sethian [18] have recently presented new algorithms for Hamilton–Jacobi and level set equations in the framework of finite element technology to be used on triangular grids. Taking advantage of the finite element formulations and the geometrical flexibility of triangular meshes, Barth and Sethian [18] use adaptive mesh refinement strategies to improve the accuracy and the computational efficiency of the algorithms. Mesh adaptivity, but in quadrilateral grids, is also used by Strain [11] to solve level set equations with a time stepping semi-Lagrangian formulation. More recently, References [19, 20] propose the combination of the level set method with finite elements for two-phase flows; Chessa and Belytschko [19] uses an extended finite-element method and Quecedo and Pastor [20] applies the characteristic based scheme of Reference [21].

Due to some well known advantages of the semi-Lagrangian schemes in dealing with advection dominated flows, see for instance References [10, 22, 23] and the references therein, we also propose a semi-Lagrangian scheme for time discretization of the material derivative $\mathrm{D}/\mathrm{D}t$ in the Navier–Stokes equations as well as in the level set and reinitialization equations, combined with mixed finite elements for the Navier–Stokes equations and linear finite elements for the level set function.

### 4.1. Time discretization for the Navier–Stokes and level set equations

To apply the semi-Lagrangian scheme for time discretization of the material derivative of (1) and (9) we divide the time interval $[0, T]$ into $N$ small intervals $I_n = [t_n, t_{n+1}]$, $0 \leqslant n \leqslant N-1$, of equal length $\Delta t$. Then, we integrate (1) and (9) along the characteristics $X(x, t_{n+1}; t)$ of the operator (2) which satisfy the system of ordinary differential equations

$$\begin{aligned} \frac{\mathrm{d}X(x, t_{n+1}; t)}{\mathrm{d}t} &= \mathbf{u}(X(x, t_{n+1}; t), t), \quad t \in [t_n, t_{n+1}), \quad x \in D \\ X(x, t_{n+1}; t_{n+1}) &= x \end{aligned} \tag{28}$$

For a given time instant $t \in [t_n, t_{n+1})$, $X(x, t_{n+1}; t)$ denotes the coordinates of the point whose coordinates at time $t_{n+1}$ are $x$, or in other words, $X(x, t_{n+1}; t)$ is the position at instant $t$ of a particle moving with the flow velocity $\mathbf{u}$ that will arrive at point $x$ at instant $t_{n+1}$. Thus, integrating (9) and (1) along the characteristics in the interval $[t_n, t_{n+1})$, it follows that for all $x \in D$

$$\int_{t_n}^{t_{n+1}} \frac{\mathrm{D}\phi(X(x, t_{n+1}; t), t)}{\mathrm{D}t}\, \mathrm{d}t = 0 \implies \phi(x, t_{n+1}) = \phi(X(x, t_{n+1}; t_n), t_n) \tag{29}$$

and

$$\int_{t_n}^{t_{n+1}} \frac{\mathrm{D}(\rho_\alpha(\phi)\mathbf{u})(X(x,t_{n+1};t),t)}{\mathrm{D}t}\,\mathrm{d}t = -\int_{t_n}^{t_{n+1}} \nabla p(X(x,t_{n+1};t),t)\,\mathrm{d}t$$

$$+\int_{t_n}^{t_{n+1}} \nabla\cdot[(\rho_\alpha(\phi)v_\alpha(\phi)\nabla\mathbf{u})(X(x,t_{n+1};t),t)]\,\mathrm{d}t$$

$$+\int_{t_n}^{t_{n+1}} \mathbf{F}(X(x,t_{n+1};t),.t)\,\mathrm{d}t \qquad (30)$$

Adapting the scheme derived by Allievi and Bermejo [12] to (30), we propose the following time discretization scheme for computing a numerical solution to (1) and (9).

We postpone to Section 4.3.1 the description of the method to calculate steps (1.1) ($X(x,t_{n+1};t_n)$) (1.2) and (1.3), that is, $\overline{\mathbf{u}}^n(x)$ and $\overline{\phi}^n(x)$, respectively, in a finite element space.

*Scheme 1*

Given $\mathbf{u}_0(x)$ and $\phi(x,0)$ (Equation (10)), for any $x\in D$ and for $n=0,1,\dots,N-1$, do:

(1.1) calculate $X(x,t_{n+1};t_n)$;

(1.2) calculate $\mathbf{u}^n(X(x,t_{n+1};t_n))$ and set $\overline{\mathbf{u}}^n(x)=\mathbf{u}^n(X(x,t_{n+1};t_n))$;

(1.3) calculate $\overline{\phi}^n(x)=\phi^n(X(x,t_{n+1};t_n))$, set $\phi^{n+1}(x)=\overline{\phi}^n(x)$ and GO TO scheme 2 for the reinitialization of $\phi^{n+1}(x)$.

(1.4) Solve

$$\rho_\alpha(\phi^{n+1})\mathbf{u}^{n+1} - \frac{\Delta t}{2}\nabla\cdot(\rho_\alpha(\phi^{n+1})v_\alpha(\phi^{n+1})\nabla\mathbf{u}^{n+1}) + \Delta t\nabla p^{n+1}$$

$$= \rho_\alpha(\phi^{n+1})\overline{\mathbf{u}}^n + \frac{\Delta t}{2}\nabla\cdot(\rho_\alpha(\phi^{n+1})v_\alpha(\phi^{n+1})\nabla\overline{\mathbf{u}}^n) + \Delta t\rho_\alpha(\phi^{n+1})g\nabla z$$

$$+\frac{\Delta t}{2}(\mathbf{f}^{n+1}(x) + \mathbf{f}^n(X(x,t_{n+1};t_n))) \qquad (31)$$

$$\nabla\cdot\mathbf{u}^{n+1} = 0$$

subjected to the boundary conditions (4),(5) and (6).

Some remarks are now in order. The key steps of Scheme 1 are Steps (1.1) and (1.3) because, if desired, Step (1.4) can be substituted by any stable Eulerian time discretization scheme for the Navier–Stokes equations. However, for the level set equation we advocate advantages of our quasi-monotone semi-Lagrangian scheme, such as the positivity and the unconditional stability together with the ability to manage fronts and solutions that hold strong gradients in some regions of the domain.

### *4.2. Time discretization for the reinitialization equations*

The solution $\phi^{n+1}(x)$ to (29) is not a signed distance function but one can argue, see References [9, 17], that if $\phi^n(x)$ (the initial condition for (29)) is a signed distance function and $\Delta t$ is sufficiently small, then $\phi^{n+1}(x)$ will be close to a signed distance function and, therefore, the integration period for the solution to (23) to reach the steady state, which is a signed distance function, will be small. This means that the method of characteristics can be used [16] to calculate such a steady state and, consequently, it makes sense to apply the semi-Lagrangian time discretization to compute the numerical solution to (23). We recall that rather than solving (23) we have to solve (25) to conserve the volume of fluid, so that we let $[0, \hat{\tau}]$ be the time integration interval for (25) and $N_\tau$ be the number of time steps of length $\Delta\tau$ such that $N_\tau \Delta\tau = \hat{\tau}$. In practice, one chooses $\hat{\tau}$ as $\hat{\tau} = K\alpha$, $\alpha$ being the semi-width of the transition region and $K$ a low positive integer. The semi-Lagrangian discretization of (25) is done through the following Scheme 2.

*Scheme 2* (*Semi-Lagrangian scheme for level set reinitialization*)

Given $\phi^n(x)$ (level set solution of (9) at $t_n$) and replacing sign($\phi$), $H(\phi)$ and $f(\phi)$ by their corresponding regularized formulae $\text{sign}_\alpha(\phi)$, $H_\alpha(\phi)$ and $f_\alpha(\phi)$, respectively, then for any $x \in D$ and for $m = 0, 1, \ldots, N_\tau$ do:

(2.1) Calculate $X^{\mathbf{w}}(x, \tau_{m+1}; \tau_m)$ solution at $\tau = \tau_m$ of

$$\frac{\mathrm{d}X^{\mathbf{w}}(x, \tau_{m+1}; \tau)}{\mathrm{d}\tau} = \mathbf{w}(X^{\mathbf{w}}(x, \tau_{m+1}; \tau), \tau), \quad \tau \in [\tau_m, \tau_{m+1}), \quad x \in D$$
$$X^{\mathbf{w}}(x, \tau_{m+1}; \tau_{m+1}) = x \tag{32}$$

(2.2) Calculate $d^m(X^{\mathbf{w}}(x, \tau_{m+1}; \tau_m))$ and set $\bar{d}^m(x) = d^m(X^{\mathbf{w}}(x, \tau_{m+1}; \tau_m))$,

(2.3) Calculate

$$\tilde{d}^{m+1}(x) = \bar{d}^m(x) + \Delta\tau\, \text{sign}_\alpha(\phi^n(x)) \tag{33}$$

(2.4) Following Reference [16], approximate $f_\alpha(d)$ by

$$f_a(\phi^n) = H'_\alpha(\phi^n)|\nabla\phi^n| \tag{34}$$

and calculate the Lagrange multiplier as

$$\lambda = \frac{-\int_D H'_\alpha(\phi^n)\dfrac{\tilde{d}^{m+1}(x) - \phi^n(x)}{\Delta\tau}\,\mathrm{d}x}{\int_D H'_\alpha(\phi^n) f_\alpha(\phi^n)\,\mathrm{d}x} \tag{35}$$

(2.5) Then, calculate

$$d^{m+1}(x) = \tilde{d}^{m+1}(x) + \Delta\tau\lambda f_\alpha(\phi^n) \tag{36}$$

(2.6) When $m = N_\tau - 1$, set (the new level set function at $t = t_{n+1}$)

$$\phi^{n+1}(x) = d^{m+1}(x) \tag{37}$$

(2.7) Then, GO TO step 4 of Scheme 1.

Note that by (37) we replace a non-distance level set function at time $t_n$ by a level set function that is a distance. Also, it is worth noting that (34) and (35) guarantee that [16]

$$\int_D H_\alpha(\phi^n)\,\mathrm{d}x = \int_D H_\alpha(d^{m+1})\,\mathrm{d}x$$

### 4.3. *Space discretization. Finite element formulation*

Our next concern is to formulate a space discretization of Schemes 1 and 2 in order to get the full approximation of the equations. For the space discretization we employ the finite element method. See, for instance References [15, 24] for a rigorous presentation of the method and References [25, 26] for a more readable account of the theory and practice of the finite element method for partial differential equations. Given $h_0$, $0<h_0<1$, let $h$ be a space discretization parameter such that $0<h<h_0$, we generate a regular partition $D_h$ in $\overline{D}$ of elements $T_j$ that satisfy the following conditions: (i) Let NE be the number of elements of $D_h$ and let $J=\{1,2,\ldots,\mathrm{NE}\}$ be an index set, then $\overline{D}=\cup_{j\in J}T_j$. (ii) For $j,l\in J$, $j\neq l$

$$T_j\cap T_l=\begin{cases}P_i & \text{a mesh point, or}\\ \gamma_{jl} & \text{a common boundary, or}\\ \emptyset & \text{empty set}\end{cases}$$

(iii) There exists a positive constant $\kappa$ such that for all $j\in J$, $\frac{h_j}{d_j}<\kappa$, where $d_j$ is the diameter of the sphere (circle in 2D) inscribed in $T_j$ and $h_j$ ($h_j\leqslant h$) is the largest side of $T_j$. The elements $T_j$ of the partition $D_h$ will be either simpleces or quadrilaterals (in 2 or 3 dimensions). Associated with the partition $D_h$ there exist families of finite dimensional subspaces in which we approximate the numerical solution. To describe such families we consider an element of reference $\widehat{T}\subset\mathbf{R}^{\xi}$ ($\xi$ is the space dimension) such that for each element $T_j$ of the partition $D_h$ we can define a one-to-one mapping $F_j:\widehat{T}\to T_j$. Let $\widehat{R}_s(\widehat{T})$ be the set of polynomials $\widehat{p}(\widehat{x})$ of degree $\leqslant s$ defined on $\widehat{T}$, then for each $T_j$ we define the set

$$R_s(T_j)=\{p(x),x\in T_j:\ p(x)=\widehat{p}(F_j^{-1}(x))\}\tag{38}$$

Note that in the conventional literature of finite elements, $\widehat{R}_s(\widehat{T})$ is $P_s(\widehat{T})$ if the elements of $D_h$ are $\xi$-simpleces, whereas $\widehat{R}_s(\widehat{T})$ is $Q_s(\widehat{T})$ if the elements of $D_h$ are $\xi$-quadrilaterals. To approximate the solution $(\mathbf{u},p)$ we use the Taylor–Hood element $P_2/P_1$-quadratic polynomials for velocity and linear polynomials for pressure (or $Q_2/Q_1$—biquadratic polynomials for velocity and bilinear polynomials for pressure). See Figures 2 and 3. Thus, we are in a condition to define the finite element spaces for velocity and pressure as follows.

*Finite element spaces for velocity and pressure*

$$\begin{aligned}\mathbf{V}_h&=\{\mathbf{v}_h\in(C^0(\overline{D}))^{\xi}:\mathbf{v}_h|_{T_j}\in(R_2(T_j))^{\xi},1\leqslant j\leqslant\mathrm{NE}\}\\ Q_h&=\{q_h\in C^0(\overline{D}):q_h|_{T_j}\in R_1(T_j),1\leqslant j\leqslant\mathrm{NE}\}\\ \mathbf{V}_{h0}&=\{\mathbf{v}_h\in\mathbf{V}_h:\mathbf{v}_h|_{\Gamma_i^s}=0,(i=1,2)\}\end{aligned}\tag{39}$$

where $C^0(\overline{D})$ denotes the space of continuous and bounded functions in $D$. If the boundary condition for velocity is only Dirichlet homogeneous, see (4), then we shall also consider the space

$$S_h=Q_h\cap L_0^2\tag{40}$$

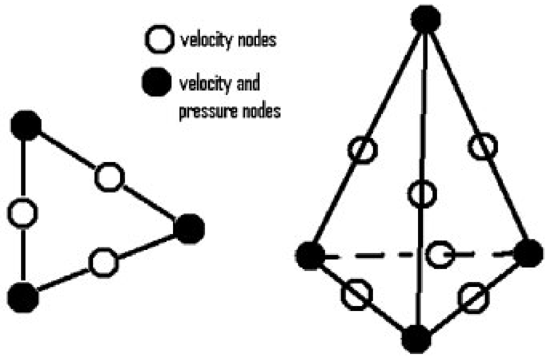

Figure 2. $P_2/P_1$ Taylor–Hood elements.

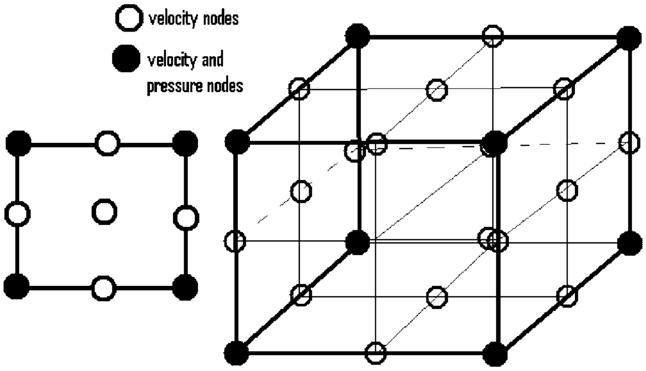

Figure 3. $Q_2/Q_1$ Taylor–Hood elements.

where

$$L_0^2 = \left\{ q \in L^2(D) : \int_D q \, \mathrm{d}x = 0 \right\} \tag{41}$$

These spaces possess properties that guaranty the stability and convergence of the approximate solution. See References [27, 28].

($A1$) *Inf-sup property*: There exists a positive constant $\beta$ independent of $h$ such that

$$\inf_{q_h \in Q_h} \sup_{u_h \in V_h} \frac{b(u_h, q_h)}{\|u_h\|_1} \geqslant \beta \|q_h\|$$

where the bilinear form $b: V_{h0} \times Q_h \to \mathbf{R}$ is defined by

$$b(u_h, q_h) = -\int_D q_h \nabla \cdot u_h \, \mathrm{d}x$$

(*A*2) *Approximation property*: For all $\mathbf{u} \in (H^{r+1}(D))^{\xi}, q \in H^r(D)/\mathbf{R}$, $1 \leqslant r \leqslant m$, there exist positive constants $K$ such that

$$\inf_{u_h \in V_h} \{\|u - u_h\| + h\|u - u_h\|_1\} \leqslant K h^{r+1} \|u\|_{r+1}$$

and

$$\inf_{q_h \in Q_h} \|q - q_h\| \leqslant K h^r \|q\|_{H^r/\mathbf{R}}$$

In the above relations we have used the Hilbert spaces $L^2(D)$, $H^{m+1}(D)$ and $H^r(D)/\mathbf{R}$ whose norms are denoted by $\|\cdot\|$, $\|\cdot\|_{m+1}$ and $\|\cdot\|_{H^r(D)/\mathbf{R}}$, respectively. See Section 5 for a definition of these spaces.

To approximate the level set function $\phi$ we use the $P_1$-iso $P_2$ (or $Q_1$-iso $Q_2$) finite element, see Figure 4, with the following discrete space.

*Finite element space for the level set function*:

$$\mathrm{LS}_h = \{\phi_h \in C^0(\overline{D}) : \phi_h|_{T_{ji}} \in P_1(T_{ji}),\ 1 \leqslant j \leqslant NE,\ 1 \leqslant i \leqslant 2^{\xi}\} \tag{42}$$

with the approximation property

$$\inf_{\phi_h \in \mathrm{LS}_h} \|\phi - \phi_h\|_l \leqslant K h^s \|q\|_r,\ s = \min(2 - l, r - l) \tag{43}$$

Let MP and MV be the number of pressure and velocity points, respectively, in the mesh, since the velocity and the level set functions share the same set of mesh points, then MV is also the number of level set points in $D_h$. We have that any $\mathbf{v}_h \in \mathbf{V}_{h0}$, $q_h \in Q_h$ and $\phi_h \in \mathrm{LS}_h$

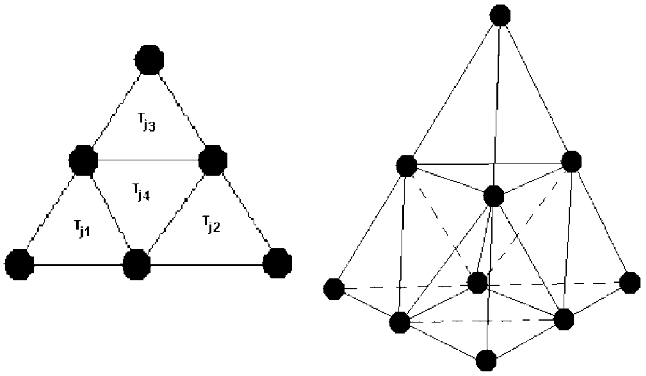

Figure 4. $P_1$-iso$P_2$ element for $\phi$.

can be represented as

$$\mathbf{v}_h = \sum_{i=1}^{\mathrm{MV}} \mathbf{V}_i \chi_i$$
$$q_h = \sum_{k=1}^{\mathrm{MP}} Q_k \varphi_k \tag{44}$$
$$\phi_h = \sum_{i=1}^{\mathrm{MV}} \Phi_i \psi_i$$

where $\{\chi_i\}_{i=1}^{\mathrm{MV}} \in \mathbf{V}_{h0}$, $\{\varphi_k\}_{k=1}^{\mathrm{MP}} \in Q_h$ and $\{\psi_i\}_{i=1}^{\mathrm{MV}} \in \mathrm{LS}_h$ are the global basis functions of $\mathbf{V}_{h0}$, $Q_h$ and $\mathrm{LS}_h$, respectively, and $\{\mathbf{V}_i\}_{i=1}^{\mathrm{MV}}$, $\{Q_k\}_{k=1}^{\mathrm{MP}}$ and $\{\Phi_i\}_{i=1}^{\mathrm{MV}}$ are the sets of nodal values of $\mathbf{v}_h$, $q_h$ and $\phi_h$, respectively. Next, we describe the implementation of the steps of Schemes 1 and 2 in a finite element framework.

*4.3.1. Computation of the departure points $X(x, t_{n+1}; t_n)$.* A crucial step for the success of the semi-Lagrangian schemes is the accurate computation of the departure points or, equivalently, the feet of the characteristics. There are a number of methods to perform such calculations, for instance, explicit Runge–Kutta schemes of order 4 or some predictor–corrector schemes of order $\geqslant 2$; however, based on the experience of Reference [8] and on our own one, we find very satisfactory the behaviour of the scheme described in Reference [12] which combines the scheme 2 of Reference [8] with the search–locate algorithm for unstructured meshes of Reference [29].

Suppose that we know the solution $\{\mathbf{u}_h^s, p_h^s, \phi_h^s\}$, $0 \leqslant s \leqslant n$, we initiate the calculations to obtain the approximate solution at $t_{n+1}$ computing the departure points that correspond to interior mesh points $\{x_i\}_{i=1}^{\mathrm{MV}^o}$. To do so, we proceed as follows.

For $i = 1, 2, \ldots, \mathrm{MV}^o$, let $X_{hi}^n := X_h(x_i, t_{n+1}; t_n)$ denote an approximation to the true departure point $X(x_i, t_{n+1}; t_n)$, compute

$$X_{hi}^n = x_i - \varepsilon_{hi} \tag{45}$$

where $\varepsilon_{hi}$ is calculated by functional iteration up to a given tolerance TOL1 as

$$\varepsilon_{hi}^{(k+1)} = \frac{\Delta t}{2}\left[3\mathbf{u}_h^n\left(x_i - \frac{1}{2}\varepsilon_{hi}^{(k)}\right) - \mathbf{u}_h^{n-1}\left(x_i - \frac{1}{2}\varepsilon_{hi}^{(k)}\right)\right], \quad k = 0, 1, \ldots \tag{46}$$

with $\varepsilon_{hi}^{(0)} = 0$. We justify in Section 5.1 formula (46). Since $\mathbf{u}_h^n$ and $\mathbf{u}_h^{n-1}$ are in $\mathbf{V}_{h0}$, we calculate $\mathbf{u}_h^n(x_i - \frac{1}{2}\varepsilon_{hi}^{(k)})$ and $\mathbf{u}_h^{n-1}(x_i - \frac{1}{2}\varepsilon_{hi}^{(k)})$ applying (44), that is

$$\mathbf{u}_h^{n-l}\left(x_i - \frac{1}{2}\varepsilon_{hi}^{(p)}\right) = \sum_{j=1}^{\mathrm{MV}} \mathbf{U}_j^{n-l} \chi_j\left(x_i - \frac{1}{2}\varepsilon_{hi}^{(p)}\right), \quad l = 0, 1 \tag{47}$$

The actual values of the weights occurring in Equation (47) are obtained in Section 5.1.

It is clear that in order to perform these finite element interpolations from the values of $\mathbf{U}^{n-l}$ at the vertices of the elements, we need to find the mesh element that contains the point $x_i - \frac{1}{2}\varepsilon_{hi}^{(k)}$. If the mesh is composed of either uniform squares or structured quadrilaterals, this is very easy to achieve and does not represent any computational burden; so that, the entire procedure, namely, location of the element and interpolation, is quick and cheap. However, in irregular meshes things are more complicated because in addition to finding the element where $x_i - \frac{1}{2}\varepsilon_{hi}^{(k)}$ is located, we also need to calculate the natural coordinates of $x_i - \frac{1}{2}\varepsilon_{hi}^{(k)}$ to do the interpolation in the element of reference . An efficient algorithm for both items, finding the element and calculating the natural coordinates, is described in Reference [29].

*4.3.2. Evaluation of functions at the departure points.* Once we have computed the set of departure points $\{X_{hi}^n\}$ and the set of elements $\{T_l\}$ where these points are located, we evaluate the velocity and the level set function at these points by the quasi-monotone interpolation algorithm proposed in Reference [14]. Thus, for $i = 1, \ldots, \mathrm{MV}^o$ consider the departure point $X_{hi}^n$ that corresponds to the interior mesh-point $x_i$, the element $T_l \ni X_{hi}^n$ and the sets of nodal values $\{\mathbf{U}_1^n, \ldots, \mathbf{U}_{\mathrm{NH}}^n\}_{T_l}$ and $\{\Phi_1^n, \ldots, \Phi_{\mathrm{NH}}^n\}_{T_l}$ of the velocity and level set functions in $T_l$, respectively. Then,

(i) calculate $\mathbf{U}_i^{*n}$ and $\Phi_i^{*n}$ as

$$\mathbf{U}_i^{*n} = \sum_{j=1}^{\mathrm{NH}} \mathbf{U}_j^n \chi_j^l(X_{hi}^n) \tag{48}$$

$$\Phi_i^{*n} = \sum_{j=1}^{\mathrm{NH}} \Phi_j^n \chi_j^l(X_{hi}^n) \tag{49}$$

where the set of basis functions $\{\chi_j^l\}_{j=1}^{\mathrm{NH}}$ is the restriction to element $T_l$ of the set of global basis functions $\{\chi_i\}_{i=1}^{\mathrm{MV}}$.

(ii) Find in the element $T_l$

$$\begin{aligned} \mathbf{U}^+ &:= \max\{\mathbf{U}_1^n, \ldots, \mathbf{U}_{\mathrm{NH}}^n\}_{T_l} \\ \mathbf{U}^- &:= \min\{\mathbf{U}_1^n, \ldots, \mathbf{U}_{\mathrm{NH}}^n\}_{T_l} \end{aligned} \tag{50}$$

and

$$\begin{aligned} \Phi^+ &:= \max\{\Phi_1^n, \ldots, \Phi_{\mathrm{NH}}^n\}_{T_l} \\ \Phi^- &:= \min\{\Phi_1^n, \ldots, \Phi_{\mathrm{NH}}^n\}_{T_l} \end{aligned} \tag{51}$$

(iii) Calculate $\overline{\mathbf{U}}_i^n$ and $\overline{\Phi}_i^n$ as

$$\overline{\mathbf{U}}_i^n = \begin{cases} \mathbf{U}^+ & \text{if } \mathbf{U}_i^{*n} > \mathbf{U}^+ \\ \mathbf{U}^- & \text{if } \mathbf{U}_i^{*n} < \mathbf{U}^- \\ \mathbf{U}_i^{*n} & \text{otherwise} \end{cases} \tag{52}$$

and

$$\overline{\Phi}_i^n = \begin{cases} \Phi^+ & \text{if } \Phi_i^{*n} > \Phi^+ \\ \Phi^- & \text{if } \Phi_i^{*n} < \Phi^- \\ \Phi_i^{*n} & \text{otherwise} \end{cases} \tag{53}$$

(iv) Set

$$\overline{\mathbf{u}}_h^n(x) = \sum_{i=1}^{\mathrm{MV}} \overline{\mathbf{U}}_i^n \chi_i(x) \tag{54}$$

$$\overline{\phi}_h^n(x) = \sum_{i=1}^{\mathrm{MV}} \overline{\Phi}_i^n \psi_i(x) \tag{55}$$

and

$$\phi_h^{n+1}(x) = \overline{\phi}_h^n(x) \tag{56}$$

The latter equation means that for all $i$, $1 \leqslant i \leqslant \mathrm{MV}^0$, $\Phi_i^{n+1} = \overline{\Phi}_i^n$.

*Remarks*

Some remarks are now in order.

(1) We should point out that although the approximate level set function $\phi_h^{n+1} \in \mathrm{LS}_h$ is a piecewise polynomial of degree 1, we calculate its values at the departure points by piecewise Lagrange interpolation of degree 2, using for this purpose the basis functions of the space $\mathbf{V}_h$. We do so for the following reason. The values that $\phi_h^n$ takes at the departure points $X_{hi}^n$ become the nodal values of $\phi_h^{n+1}$, which are the values of interest in the numerical calculations, so that, we would like to compute them as accurately as we can and with a computational cost as low as possible; however, it is well known that linear interpolation yields results whose accuracy is not sufficiently good, then we abandon linear interpolation in favour of the quadratic interpolation because in our numerical framework this is a good alternative, as considering computer cost versus accuracy.

(2) It is easy to show, see References [13, 14], that steps (ii)–(iii) amount for computing $\overline{\mathbf{U}}_i^n$ and $\overline{\phi}_i^n$ by the following formulae:

$$\begin{aligned} \overline{\mathbf{U}}_i^n &= (1 - C_i(\mathbf{u}_h^n)) R_1 \mathbf{u}_h^n(X_{hi}^n) + C_i(\mathbf{u}_h^n) R_2 \mathbf{u}_h^n(X_{hi}^n) \\ \overline{\phi}_i^n &= (1 - C_i(\phi_h^n)) R_1 \phi_h^n(X_{hi}^n) + C_i(\phi_h^n) R_2 \phi_h^n(X_{hi}^n) \end{aligned} \tag{57}$$

where $R_1$ and $R_2$ are linear and quadratic polynomial functions, respectively, defined in (38). Note that in (57) $R_1 v$ is determined by the values of $v$ at the vertices of the elements $T_j$ and the basis functions $\{\varphi_i\}_{i=1}^{\mathrm{MP}}$, and $R_2 v$ is determined by the values of $v$ at the vertices and at mid-nodes on the edges of $T_j$ and the basis functions $\{\chi_i\}_{i=1}^{\mathrm{MV}}$. $R_s \mathbf{u}_h^n(X_{hi}^n)$ and $R_s \phi_h^n(X_{hi}^n)$, $s = 1, 2$, denote the values at $X_{hi}^n$ of $R_s \mathbf{u}_h^n$ and $R_s \phi_h^n$, respectively. $C_i(\mathbf{u}_h^n)$ and $C_i(\phi_h^n)$ are limiting coefficients given by the formula

$$C_i(\phi_h^n) = \min \left( 1, \begin{cases} \dfrac{\Phi^+ - R_1 \phi_h^n(X_{hi}^n)}{P(\phi_h^n)} & \text{if } P(\phi_h^n) > 0 \\[2ex] \dfrac{\Phi^- - R_1 \phi_h^n(X_{hi}^n)}{P(\phi_h^n)} & \text{if } P(\phi_h^n) < 0 \\[2ex] 1 & \text{if } P(\phi_h^n) = 0 \end{cases} \right) \tag{58}$$

where $P(\phi_h^n)$ is defined by

$$P(\phi_h^n)=R_2\phi_h^n(X_{hi}^n)-R_1\phi_h^n(X_{hi}^n) \tag{59}$$

Analogous calculations give $C_i(\mathbf{u}_h^n)$.

*4.3.3. Fully discrete Stokes problem.* The finite element formulation of (31) is as follows. Find $(\mathbf{u}_h^{n+1},p_h^{n+1})\in\mathbf{V}_{h0}\times Q_h$ such that for any $(\mathbf{v}_h,q_h)\in\mathbf{V}_{h0}\times Q_h$

$$\int_D \rho_{\alpha h}(\phi_h^{n+1})\mathbf{u}_h^{n+1}\cdot\mathbf{v}_h\,\mathrm{d}x+\frac{\Delta t}{2}\int_D \rho_{\alpha h}(\phi_h^{n+1})v_{\alpha h}(\phi_h^{n+1})\nabla\mathbf{u}_h^{n+1}\cdot\nabla\mathbf{v}_h\,\mathrm{d}x$$

$$-\Delta t\int p_h^{n+1}\nabla\cdot\mathbf{v}_h\,\mathrm{d}x=(\mathbf{G}_h^{n+1},\mathbf{v}_h) \tag{60}$$

$$\int_D q_h\nabla\cdot\mathbf{u}_h^{n+1}\,\mathrm{d}x=0$$

where

$$(\mathbf{G}_h^{n+1},\mathbf{v}_h)=\int_D \rho_{\alpha h}(\phi_h^{n+1})\bar{\mathbf{u}}_h^n\cdot\mathbf{v}_h\,\mathrm{d}x-\frac{\Delta t}{2}\int_D \rho_{\alpha h}(\phi_h^{n+1})v_{\alpha h}(\phi_h^{n+1})\nabla\bar{\mathbf{u}}_h^n\cdot\nabla\mathbf{v}_h\,\mathrm{d}x$$

$$-\Delta t\int_D g(\rho_\alpha(\phi_h^{n+1})z)_h\nabla\cdot\mathbf{v}_h\,\mathrm{d}x-\Delta t\int_D gz_h\nabla\rho_{\alpha h}(\phi_h^{n+1})\cdot\mathbf{v}_h\,\mathrm{d}x$$

$$+\frac{\Delta t}{2}\int_D(\mathbf{f}^{n+1}(x)+\mathbf{f}^n(X(x,t_{n+1};t_n))\cdot\mathbf{v}_h\,\mathrm{d}x$$

with $\rho_{\alpha h}(\phi_h^{n+1})$ and $v_{\alpha h}(\phi_h^{n+1})\in\mathbf{V}_h$, $(\rho_\alpha(\phi_h^{n+1})z)_h$ and $z_h\in Q_h$.

We calculate the numerical solution of (60) using the Uzawa-conjugate gradient algorithm as presented in Reference [30].

*4.3.4. Fully discrete reinitialization scheme.* We describe the space discretization by finite elements of Scheme 2. We start with $f_\alpha(\phi^n)=H'_\alpha(\phi^n)|\nabla\phi^n|$ whose finite element approximation, denoted by $f_{\alpha h}(\phi_h^n)$, is taken in $\mathrm{LS}_h$. We cannot calculate the latter function as $f_{\alpha h}(\phi_h^n)=H'_\alpha(\phi_h^n)|\nabla\phi_h^n|$ because neither $H'_\alpha(\phi_h^n)$ nor $|\nabla\phi_h^n|$ are in $\mathrm{LS}_h$, as we can ascertain by noting that $H'_\alpha(\phi_h^n)$ is not a piecewise polynomial of degree 1 and recalling the fact that if the finite element approximation $\phi_h^n$ is in $\mathrm{LS}_h$ its gradient is not. We overcome this problem by defining $f_{\alpha h}(\phi_h^n)\in\mathrm{LS}_h$ as

$$f_{\alpha h}(\phi_h^n)=\sum_{i=1}^{\mathrm{MV}}f_i\psi_i \tag{61}$$

such that

$$\int_D f_{\alpha h}(\phi_h^n) b_h \, \mathrm{d}x = \int_D H'_\alpha(\phi_h^n) |\nabla \phi_h^n| b_h \, \mathrm{d}x, \quad \forall b_h \in \mathrm{LS}_h$$

Taking $b_h = \psi_i$, for $i = 1, \dots, \mathrm{MV}$, this equation leads to a linear system

$$\mathrm{MF} = B$$

where $M$ is the so-called mass matrix, with entries $m_{ij} = \int_D \psi_i \psi_j \, \mathrm{d}x$, $1 \leqslant i, j \leqslant \mathrm{MV}$, $F = [f_1, \dots, f_{\mathrm{MV}}]^{\mathrm{T}}$ and $B = [b_1, \dots, b_{\mathrm{MV}}]^{\mathrm{T}}$ with $b_i = \int_D H'_\alpha(\phi_h^n) |\nabla \phi_h^n| \psi_i \, \mathrm{d}x$. The matrix $M$ is non singular and positive definite, but $M^{-1}$ has negative entries that may cause the function $f_{\alpha h}(\phi_h^n)$ have oscillations that can spoil the positivity properties of the level set function. We avoid this by substituting $M$ by the diagonal matrix $\overline{M}$, the entries of which are $\overline{m}_{ii} = \sum_{j=1}^{\mathrm{MV}} m_{ij} = \int_D \psi_i \, \mathrm{d}x$. This makes the inversion of $M$ trivial and the coefficients $f_i$ are then given by

$$f_i = \frac{\int_D H'_\alpha(\phi_h^n) |\nabla \phi_h^n| \psi_i \, \mathrm{d}x}{\int_D \psi_i \, \mathrm{d}x} \tag{62}$$

Likewise, for each $m$ we calculate an approximation $\mathbf{w}_h \in \mathbf{LS}_h = (\mathrm{LS}_h)^\xi$ to the advection velocity

$$\mathbf{w} = \mathrm{sign}_\alpha(\phi) \frac{\nabla d}{|\nabla d|}$$

as

$$\mathbf{w}_h^{m+1} = \sum_{i=1}^{\mathrm{MV}} \mathbf{w}_i^{m+1} \psi_i \tag{63}$$

such that

$$\int_D \mathbf{w}_h^{m+1} \cdot \mathbf{b}_h \, \mathrm{d}x = \int_D \mathrm{sign}_\alpha(\phi_h^n) \frac{\nabla d_h^{m+1}}{|\nabla d_h^{m+1}|} \cdot \mathbf{b}_h \, \mathrm{d}x, \quad \forall \mathbf{b}_h \in (\mathrm{LS}_h)^p$$

$\mathbf{w}_h^{m+1}$ is then Lipschitz continuous and guarantees the uniqueness of $X_h^{\mathbf{w}m}$. From this equation we obtain the linear system of equations

$$M \mathbf{w}^{m+1} = \mathbf{r}^{m+1} \tag{64}$$

where $M$ is the mass matrix, $\mathbf{w}^{m+1} = [\mathbf{w}_1^{m+1}, \dots, \mathbf{w}_{\mathrm{MV}}^{m+1}]^{\mathrm{T}}$ and $\mathbf{r}^{m+1} = [\mathbf{r}_1^{m+1}, \dots \mathbf{r}_{\mathrm{MV}}^{m+1}]^{\mathrm{T}}$ with

$$\mathbf{r}_i^{m+1} = \int_D \mathrm{sign}_\alpha(\phi_h^n) \frac{\nabla d_h^{m+1}}{|\nabla d_h^{m+1}|} \psi_i \, \mathrm{d}x \tag{65}$$

Since the condition number of $M$ is low [26], then the calculation of the solution of (64) by the diagonal preconditioned conjugate gradient method is very fast.

The procedure to calculate $X_h^{\mathbf{w}m+1}$ is in essence the same as the one employed for $X_h^n$. Specifically, for $i = 1, 2, \dots, \mathrm{MV}$, let $X_{hi}^{\mathbf{w}m} = X_h^{\mathbf{w}}(x_i, \tau_{m+1}; \tau_m)$ denote an approximation to the true departure point $X^{\mathbf{w}}(x_i, \tau_{m+1}; \tau_m)$, we compute

$$X_{hi}^{\mathbf{w}m} = x_i - \omega_{hi} \tag{66}$$

where $\omega_{hi}$ is calculated by functional iteration up to a given tolerance TOL2 by

$$\omega_{hi}^{(k+1)} = \frac{\Delta\tau}{2}\left[3\mathbf{w}_h^m\left(x_i - \frac{1}{2}\omega_{hi}^{(k)}\right) - \mathbf{w}_h^{n-1}\left(x_i - \frac{1}{2}\omega_{hi}^{(k)}\right)\right], \quad k = 0, 1, \ldots \tag{67}$$

with $\omega_{hi}^{(0)} = 0$. Since $\mathbf{w}_h^n$ and $\mathbf{w}_h^{n-1}$ are in $\mathbf{LS}_h$, we calculate $\mathbf{w}_h^n(x_i - \frac{1}{2}\omega_{hi}^{(k)})$ and $\mathbf{w}_h^{n-1}(x_i - \frac{1}{2}\omega_{hi}^{(k)})$ applying (44), that is, $\mathbf{w}_h^{n-l}(x_i - \frac{1}{2}\omega_{hi}^{(k)}) = \sum_{j=1}^{\mathrm{MV}} \mathbf{w}_j^{n-l}\psi_j(x_i - \frac{1}{2}\omega_{hi}^{(k)})$, $l = 0$ and 1.

Next, we calculate $\bar{d}_h^m$ at $X_{hi}^{\mathbf{w}m}$ by the procedure described in Section 4.3.2. Thus,

(i) compute

$$d_i^{*m} = \sum_{j=1}^{\mathrm{NH}} d_j^m \chi_j^l(X_{hi}^{\mathbf{w}m}) \tag{68}$$

(ii) Find the element $T_l$ that contains $X_{hi}^{\mathbf{w}m}$ and set

$$\begin{aligned} d^+ &:= \max\{d_1^m, \ldots, d_{\mathrm{NH}}^m\}_{T_l} \\ d^- &:= \min\{d_1^m, \ldots, d_{\mathrm{NH}}^n\}_{T_l} \end{aligned} \tag{69}$$

$$\bar{d}_i^m = \begin{cases} d^+ & \text{if } d_i^{*m} > d^+ \\ d^- & \text{if } d_i^{*m} < d^- \\ d_i^{*m} & \text{otherwise} \end{cases} \tag{70}$$

(iii) Set

$$\bar{d}_h^m(x) = \sum_{i=1}^{\mathrm{MV}} \bar{d}_i^m \psi_i(x) \tag{71}$$

Once we have obtained $\bar{d}^m(x)$, we compute, for each $i = 1, 2, \ldots, \mathrm{MV}$, the mesh-point values of $\tilde{d}_h^{m+1}(x) \in \mathrm{LS}_h$ by

$$\tilde{d}_i^{m+1} = \bar{d}_i^m + \Delta\tau\, \mathrm{sign}_\alpha(\phi_h^n(x_i)) \tag{72}$$

We proceed now to calculate the Lagrange multiplier as

$$\lambda_h^m = \frac{-\int_D H_\alpha'(\phi_h^n)\dfrac{\tilde{d}_h^{m+1}(x) - \phi_h^n(x)}{\Delta\tau}\,\mathrm{d}x}{\int_D H_\alpha'(\phi_h^n) f_{\alpha h}(\phi_h^n)\,\mathrm{d}x} \tag{73}$$

Reference [16] recommends to approximate the integrals by high order quadrature rules; so that, we use Gaussian quadrature rules of order 4. Finally, we calculate $d_h^{m+1} \in \mathrm{LS}_h$ as

$$d_h^{m+1} = \tilde{d}_h^{m+1} + \Delta\tau\lambda_h^m f_{\alpha h}(\phi_h^n) \tag{74}$$

and when $m = N_\tau - 1$, we set the level set function at $t_n$

$$\phi_h^n(x) = d_h^{m+1}(x) \tag{75}$$

*Remarks*

(1) Note that by definition, see (61) and (62), $f_{\alpha h}(\phi_h^n)$ is zero outside the transition band $[-\alpha, \alpha]$.

(2) We calculate the integrals in (73) as

$$\int_D h(x)\,\mathrm{d}x = \sum_{j=1}^{\mathrm{NE}} \int_{T_j} h(x)\,\mathrm{d}x$$

where the integral in each element $T_j$ is approximated by a Gaussian quadrature rule as

$$\int_{T_j} h(x)\,\mathrm{d}x \simeq \sum_{k=1}^{\mathrm{GP}} \varpi_k h(x_k)$$

where $\varpi_k$ and $x_k$ are the weights and the Gaussian points in $T_j$, respectively. Since $H'_\alpha(\phi_h^n)$ is zero outside the band $[-\alpha, \alpha]$, then the elements which contribute to the integrals of (73) are those whose intersections with this band are not void. The number of such elements is low in comparison with the total number of elements in $D$, so that the calculation of the multiplier is very fast.

## 5. NUMERICAL ANALYSIS

It is outside the scope of this paper to give a detailed numerical analysis of the method; however, we consider necessary to provide some basic theoretical results that will help to explain its performance. Specifically, we shall study the stability for the fully discrete Navier–Stokes equations (60) and discrete level set function (56), as well as the convergence of the approximate feet of the characteristics $X_h^n$. Before going into the details and for completeness, we introduce some notation on functional spaces we need below. We restrict ourselves to real value functions. For $1 \leqslant p < \infty$, $L^p(D)$ denotes the space of functions $u$ such that $|u|^p$ is Lebesgue integrable in $D$. $L^p(D)$ is a Banach space with the norm

$$\|u\|_{L^p(D)} = \left( \int |u|^p \,\mathrm{d}x \right)^{1/p}$$

When $p = \infty$, $L^\infty(D)$ is the space of functions that are bounded and locally Lebesgue integrable in $D$. It is also a Banach space with norm

$$\|v\|_{L^\infty(D)} = \inf\{\sup\{|v(x)| : x \in D \backslash A\}\}\text{A: is a set of measure zero}$$

For $m$ integer $\geqslant 1$, $\alpha = (\alpha_1, \ldots, \alpha_\xi)$, with $0 \leqslant \alpha_l \leqslant m$ for $1 \leqslant l \leqslant \xi$ and $|\alpha| = \alpha_1 + \cdots + \alpha_\xi$, $D^\alpha v = \frac{\partial v^{|\alpha|}}{\partial x_1^{\alpha_1} \ldots \partial x_d^{\alpha_\xi}}$. The Sobolev spaces $W^{m,p}(D)$ are defined as

$$W^{m,p}(D) = \{v \in L^p(D) : D^\alpha v \in L^p(D), |\alpha| \leqslant m, 1 \leqslant p < \infty\}$$

where $D^{\alpha}v$ are weak derivatives. The space $W^{m,p}(D)$ are Banach spaces with norms

$$\|v\|_{W^{m,p}(D)} = \left( \sum_{|\alpha| \leqslant m} \|D^{\alpha}v\|_{L^p(D)} \right)^{1/p}$$

$$\|v\|_{W^{m,\infty}(D)} = \max_{|\alpha| \leqslant m} \|D^{\alpha}v\|_{L^{\infty}(D)}$$

When $p=2$, $W^{m,p}(D)$ coincides with the Hilbert space $H^m(D)$. Notice that when $p=2$, we write the norms of the Hilbert spaces $L^2$ and $H^m$ as $\|\cdot\|$ and $\|\cdot\|_m$, respectively. We require spaces that incorporate time dependency. Let $X$ be any of the spaces introduced above, if $v(x,t)$ is a function defined on $D \times [0,T]$ the following norms are used:

$$\|v\|_{L^p([0,T];X)} = \left( \int_0^{\mathrm{T}} \|v(t)\|_X^p \,\mathrm{d}t \right)^{1/p} \qquad 1 \leqslant p < \infty$$

$$\|v\|_{L^{\infty}([0,T];X)} = \inf\{\sup\{\|v(t)\|_X : t \in [0,T]\backslash I\} : I \text{ a set of measure zero}\}$$

The space $L^p([0,T];X)$ is the set of functions $v$ such that the above norm is finite.

### 5.1. Error estimates for the feet $X_h^n$

An important point for the overall accuracy of the semi-Lagrangian schemes is the accurate computation of the departure points $X_{hi}^n$. We prove that the numerical procedure of Equations (45)–(47) yields a second-order error estimate for $X_{hi}^n$. We note that for all $x \in D$ and for all $n$, (28) yields

$$X(x,t_{n+1};t_n) = x - \int_{t_n}^{t_{n+1}} \mathbf{u}(X(x,t_{n+1},t),t)\,\mathrm{d}t \tag{76}$$

By analogy with (45), let us define

$$\varepsilon(x,t_{n+1};t_n) := x - X(x,t_{n+1};t_n) \tag{77}$$

and approximate the integral in (76) by the mid-point quadrature rule to obtain, assuming that $\mathbf{u}$ is sufficiently regular, that

$$\varepsilon(x,t_{n+1};t_n) = \Delta t\mathbf{u}\left( X\left( x,t_{n+1};t_n + \frac{\Delta t}{2} \right), t_n + \frac{\Delta t}{2} \right) + O(\Delta t^3) \tag{78}$$

where $(X(x,t_{n+1};t_n + \frac{\Delta t}{2}), t_n + \frac{\Delta t}{2})$ is the mid-point of the arch joining the points $(x,t_{n+1})$ and $(X(x,t_{n+1};t_n),t_n)$. By a Taylor expansion it follows that

$$X\left( x,t_{n+1};t_n + \frac{\Delta t}{2} \right) = x - \frac{1}{2}\varepsilon(x,t_{n+1};t_n) + O(\Delta t^2)$$

Substituting this expression in (78) and doing a new Taylor expansion yields

$$\varepsilon(x, t_{n+1}; t_n) = \Delta t \mathbf{u}\left(x - \frac{1}{2}\,\varepsilon(x, t_{n+1}; t_n), t_n + \frac{\Delta t}{2}\right) + O(\Delta t^3) \tag{79}$$

Since the velocity values are known at time instants $t_n$ but not at $t_n + \frac{\Delta t}{2}$, we approximate $\mathbf{u}(\cdot, t_n + \frac{\Delta t}{2})$ up to second-order by the formula

$$\mathbf{u}\left(\cdot, t_n + \frac{\Delta t}{2}\right) = \frac{1}{2}(3\mathbf{u}(\cdot, t_n) - \mathbf{u}(\cdot, t_{n-1})) + O(\Delta t^2)$$

Hence, we can express $\varepsilon(x, t_{n+1}; t_n)$ in terms of known velocity values as

$$\varepsilon = \frac{\Delta t}{2}\left(3\mathbf{u}\left(x - \frac{1}{2}\varepsilon, t_n\right) - \mathbf{u}\left(x - \frac{1}{2}\varepsilon, t_{n-1}\right)\right) + O(\Delta t^3) \tag{80}$$

By virtue of (46) and (45) we approximate $\varepsilon(x, t_{n+1}; t_n)$ and $X(x, t_{n+1}; t_n)$ as

$$\varepsilon_h = \frac{\Delta t}{2}\left(3\mathbf{u}_h\left(x - \frac{1}{2}\varepsilon_h, t_n\right) - \mathbf{u}_h\left(x - \frac{1}{2}\varepsilon_h, t_{n-1}\right)\right) \tag{81}$$

and

$$X_h(x, t_{n+1}; t_n) = x - \varepsilon_h \tag{82}$$

So that, given $\Delta t \in (0, \Delta t^*)$, $0 < \Delta t^* < 1$, if for each interval $[t_n, t_{n+1}]$ we define the error in the approximation of the feet of the characteristics as

$$e^n = X^n - X_h^n \tag{83}$$

it follows by virtue of (80) that

$$e^n = \varepsilon_h(x, t_{n+1}; t_n) - \varepsilon(x, t_{n+1}; t_n) = \frac{\Delta t}{2}\left[3\left(\mathbf{u}_h\left(x - \frac{1}{2}\varepsilon_h, t_n\right) - \mathbf{u}\left(x - \frac{1}{2}\varepsilon, t_n\right)\right)\right.$$
$$\left. - \left(\mathbf{u}_h\left(x - \frac{1}{2}\varepsilon_h, t_{n-1}\right) - \mathbf{u}\left(x - \frac{1}{2}\varepsilon, t_{n-1}\right)\right)\right]$$

Considering that

$$\mathbf{u}_h(x - \tfrac{1}{2}\varepsilon_h, \cdot) - \mathbf{u}(x - \tfrac{1}{2}\varepsilon, \cdot) = \mathbf{u}_h(x - \tfrac{1}{2}\varepsilon_h, \cdot) - \mathbf{u}(x - \tfrac{1}{2}\varepsilon_h, \cdot)$$
$$+\mathbf{u}(x - \tfrac{1}{2}\varepsilon_h, \cdot) - \mathbf{u}(x - \tfrac{1}{2}\varepsilon, \cdot)$$

and by a Taylor expansion with integral remainder

$$\mathbf{u}\left(x - \frac{1}{2}\varepsilon_h, \cdot\right) - \mathbf{u}\left(x - \frac{1}{2}\varepsilon, \cdot\right) = \frac{1}{2}(\varepsilon - \varepsilon_h) \cdot \int_0^1 \nabla\mathbf{u}(\bar{x}(z), \cdot)\,\mathrm{d}z$$

where $\bar{x}(z) = (x - \frac{1}{2}\varepsilon_h)z + (x - \frac{1}{2}\varepsilon)(1 - z)$, $0 < z < 1$, and assuming that $L = |\nabla \mathbf{u}|_{L^\infty(0,T;D)}$ is bounded a.e., we can set

$$|e^n| \leqslant \frac{3\Delta t}{2}\left|\left(\mathbf{u}_h\left(x - \frac{1}{2}\varepsilon_h, t_n\right) - \mathbf{u}\left(x - \frac{1}{2}\varepsilon_h, t_n\right)\right)\right| \\ + \frac{\Delta t}{2}\left|\left(\mathbf{u}_h\left(x - \frac{1}{2}\varepsilon_h, t_{n-1}\right) - \mathbf{u}\left(x - \frac{1}{2}\varepsilon_h, t_{n-1}\right)\right)\right| + \frac{\Delta t}{2}|e^n|L + C_1\Delta t^3$$

where $C_1$ is a bounded constant independent of $\Delta t$ and $h$. Taking $\Delta t$ sufficiently small such that $\frac{1}{2}L\Delta t < 1$ it follows that

$$|e^n| \leqslant \frac{\Delta t}{2\left(1 - \dfrac{\Delta t}{2}L\right)}(3|\mathbf{u}_h^n - \mathbf{u}^n| + |\mathbf{u}_h^{n-1} - \mathbf{u}^{n-1}| + C_1\Delta t^2)$$

Hence

$$\max_n \|e^n\| \leqslant C\Delta t\left(\max_n \|\mathbf{u}_h^n - \mathbf{u}^n\| + \Delta t^2\right) \tag{84}$$

where $C = C_1/2(1 - \frac{\Delta t^*}{2}L)$.

Note that we obtain (84) by assuming that $\varepsilon_h$ is computed exactly; however, by virtue of (46) $\varepsilon_h$ is calculated via an iterative process. So that, it remains to know the conditions for the convergence of such a process. To do so, we denote by $k$ the iteration index, $k = 1, 2, \ldots$, and set

$$e_{\text{iter}}^{(k)} := \varepsilon_h - \varepsilon_h^{(k)}$$

where (see (46))

$$\varepsilon_h^{(k)} = \frac{\Delta t}{2}\left(3\mathbf{u}_h^n\left(x - \frac{\varepsilon_h^{(k-1)}}{2}\right) - \mathbf{u}_h^{n-1}\left(x - \frac{\varepsilon_h^{(k-1)}}{2}\right)\right)$$

with

$$\varepsilon_h^{(0)} = \frac{\Delta t}{2}(3\mathbf{u}_h^n(x) - \mathbf{u}_h^{n-1}(x))$$

A Taylor expansion yields

$$\|e_{\text{iter}}^{(k)}\|_{L^\infty(D)} \leqslant \tfrac{1}{2}\Delta t\|\nabla \mathbf{u}_h^n\|_{L^\infty(D)}\|e_{\text{iter}}^{(k-1)}\|_{L^\infty(D)}$$

Hence, the procedure (46) converges to $\varepsilon_h$ if

$$\Delta t \|\nabla \mathbf{u}_h^n\|_{L^\infty(D)} < 2$$

Notice that this condition is the discrete analogue of the continuous condition $\frac{1}{2}L\Delta t < 1$ used above in the estimate for $e^n$. We summarize this analysis in the following lemma.

*Lemma 1*
Suppose that the following assumptions hold:

(1) $\mathbf{u} \in L^\infty(0, T; (W^{1,\infty}(D))^d)$;
(2) for all $n$, $\Delta t \max(\|\nabla u_h^n\|_{L^\infty(D)}, \|\nabla u^n\|_{L^\infty(D)}) < 2$;
(3) $\frac{D^2\mathbf{u}}{Dt^2} \in L^2(0, T; (L^2(D)^d)$.

Then an error estimate for the feet of the characteristics is given by

$$\max_n \|X^n - X_h^n\| \leqslant C\Delta t \left( \max_n \|\mathbf{u}_h^n - \mathbf{u}^n\| + \Delta t^2 \right)$$

## 5.2. Stability

First, we study the stability of the semi-Lagrangian advection scheme with quasi-monotone interpolation when the scheme is applied to a pure transport equation such as (9). To this end we introduce the discrete $L^\infty$-norm in both $\mathrm{LS}_h$ and $\mathbf{V}_{h0}$ defined as follows. For any $w_h \in \mathrm{LS}_h$ and $\mathbf{v}_h \in \mathbf{V}_{h0}$, $\|w_h\|_{h,\infty} = \max_j |W_j|$ and $\|\mathbf{v}_h\|_{h,\infty} = \max_j |\mathbf{V}_j|$, $1 \leqslant j \leqslant \mathrm{MV}$, respectively. We notice that discrete and continuous $L^\infty$-norms are equivalent. This is easy to see by using the corresponding definitions and elementary properties of the finite element spaces and norms. Thus, for finite element spaces whose elements are $P_1$ (or $Q_1$)-elements the discrete and continuous $L^\infty$ norms satisfy $\|w_h\|_{h,\infty} = \|w_h\|_{L^\infty(D)}$; whereas for those spaces whose elements are $P_2$ (or $Q_2$)-elements there are constant $c_1$ and $c_2$ such that $c_2\|w_h\|_{L^\infty(D)} \leqslant \|w_h\|_{h,\infty} \leqslant c_1\|w_h\|_{L^\infty(D)}$. We have the following result.

*Lemma 2*
Suppose that the assumptions of Lemma 1 hold. Then, the semi-Lagrangian scheme with quasi-monotone interpolation as described in Sections 4.3.1 and 4.3.2 is unconditionally stable in the $L^\infty$–norm when it is applied to calculate the numerical solution of an advection equation. Specifically, for all $n$ we have that

$$\|\phi_h^{n+1}\|_{h,\infty} = \|\overline{\phi}_h^n\|_{h,\infty} \leqslant \|\phi_h^n\|_{h,\infty} \leqslant \cdots \leqslant \|\phi_h^0\|_{h,\infty} \tag{85}$$

*Proof*
Let the level set function $\phi_h^n$ be the approximate solution of the pure transport problem (9)–(10). We have that

$$\phi_h^n(x) = \sum_{i=1}^{\mathrm{MV}} \Phi_i^n \psi_i(x) \quad \text{and}$$

$$\phi_h^{n+1}(x) = \sum_{i=1}^{\mathrm{MV}} \Phi_i^{n+1} \psi_i(x) = \sum_{i=1}^{\mathrm{MV}} \overline{\Phi}_i^n \psi_i(x) = \overline{\phi}_h^n$$

where the values $\overline{\Phi}_i^n$ are calculated by the quasi-monotone quadratic interpolation (48)–(56) described in Section 4.3.2. Let $l$ and $j$ be the indices such that $\|\phi_h^n\|_{h,\infty}=|\phi_l^n|$ and $\|\overline{\phi}_h^n\|_{h,\infty}=|\overline{\phi}_j^n|$, respectively. By construction of the quasi-monotone interpolation $|\overline{\phi}_j^n|\leqslant|\phi_l^n|$; so that, $\|\overline{\phi}_h^n\|_{h,\infty}\leqslant\|\phi_h^n\|_{h,\infty}$, or equivalently, $\|\phi_h^{n+1}\|_{h,\infty}\leqslant\|\phi_h^n\|_{h,\infty}$. Since this is true for all $n$, (notice that $\phi_h^n$ is solution of a pure transport problem) then it follows that $\|\phi_h^{n+1}\|_{h,\infty}\leqslant\|\phi_h^0\|_{h,\infty}$. Given that for all $n$, $\phi_h^n\in\mathrm{LS}_h$, the elements of which are $P_1-$elements, then $\|\phi_h^{n+1}\|_{L^\infty(D)}\leqslant\|\phi_h^n\|_{L^\infty(D)}\leqslant\cdots\leqslant\|\phi_h^0\|_{L^\infty(D)}$. This means that $\|\phi_h^{n+1}\|_{L^\infty(D)}$ is uniformly bounded for all $n$.

As for the estimates $\|\overline{\mathbf{u}}_h^n\|_{h,\infty}$ and $\|\overline{\mathbf{u}}_h^n\|$, applying the same arguments as above we have that for all $n$

$$\begin{aligned}&\|\overline{\mathbf{u}}_h^n\|_{h,\infty}\leqslant\|\mathbf{u}_h^n\|_{h,\infty}\quad\text{and}\\&\|\overline{\mathbf{u}}_h^n\|\leqslant C_1\|\overline{\mathbf{u}}_h^n\|_{h,\infty}\leqslant C_1\|\mathbf{u}_h^n\|_{h,\infty}\end{aligned}\tag{86}$$

We now study the stability of the Navier–Stokes solution $(\mathbf{u}_h^n, p_h^n)$. For simplicity we take $\mathbf{f}=0$. We have the following result.

*Theorem 1*

Suppose (A1) and Lemma 2 hold. Then, there exists a positive constant $C$ independent of $\Delta t$ and $h$ such that for all $n=1,2,\dots$

$$\left\|\sqrt{\rho_{\alpha h}(\phi_h^{n+1})}\mathbf{u}_h^{n+1}\right\|\leqslant\left\|\sqrt{\rho_{\alpha h}(\phi_h^{n+1})}\overline{\mathbf{u}}_h^n\right\|+\Delta tC\left\|\sqrt{\rho_{\alpha h}(\phi_h^{n+1})}gz_h\nabla\log\rho_{\alpha h}(\phi_h^{n+1})\right\|\tag{87}$$

*Proof*

We recall that $(\mathbf{u}_h^{n+1}, p_h^{n+1})$ is solution of (60). Introducing the operator $A_h: V_{h0}\to V_{h0}$ such that for all $\mathbf{v}_h\in\mathbf{V}_{h0}$

$$(A_h\mathbf{u}_h,\mathbf{v}_h)=\int_D\rho_{\alpha h}(\phi)v_{\alpha h}(\phi)\nabla\mathbf{u}_h\cdot\nabla\mathbf{v}_h\,\mathrm{d}x\tag{88}$$

and the operator $B_h:\mathbf{V}_{h0}\to Q_h$ such that for all $q_h\in Q_h$

$$(B_h\mathbf{u}_h,q_h)=b(\mathbf{u}_h,q_h)=-\int q_h\nabla\cdot\mathbf{u}_h\,\mathrm{d}x\tag{89}$$

with transpose $B_h^{\mathrm{T}}:Q_h\to\mathbf{V}_{h0}$ satisfying the relations

$$(B_h\mathbf{u}_h,q_h)=(\mathbf{u}_h,B_h^{\mathrm{T}}q_h)=b(\mathbf{u}_h,q_h)$$

It is easy to see that to find the solution of (60), with $\mathbf{f}=0$, is equivalent (in the discrete sense) to calculate the solution $(\mathbf{u}_h^{n+1}, p_h^{n+1}) \in \mathbf{V}_{h0} \times Q_h$ that satisfies the operator equation

$$\begin{aligned}
&\rho_{\alpha h}(\phi_h^{n+1})\mathbf{u}_h^{n+1} + \frac{\Delta t}{2} A_h \mathbf{u}_h^{n+1} + \Delta t B_h^{\mathrm{T}} p_h^{n+1} \\
&\quad = \rho_{\alpha h}(\overline{\phi}_h^n)\overline{\mathbf{u}}_h^n - \frac{\Delta t}{2} A_h \overline{\mathbf{u}}_h^n - \Delta t B_h^{\mathrm{T}} g(\rho_{\alpha h}(\phi_h^{n+1})z)_h - \Delta t g z_h \nabla \rho_{\alpha h}(\phi_h^{n+1})
\end{aligned} \tag{90}$$

$$B_h \mathbf{u}_h^{n+1} = 0$$

The operator $A_h$ is a self-adjoint positive definite operator with (by the compact imbedding of $H^1(D)$ in $L^2(D)$ and the Lax–Milgram theorem [31]) a compact inverse $A_h^{-1}$; so that, the eigenvalue problem: *find* $(\Omega, \lambda), \Omega \in \mathbf{V}_{h0}, \lambda$ *real, such that for all* $\mathbf{v}_h \in \mathbf{V}_{h0}$

$$(A_h \Omega, \mathbf{v}_h) = \lambda(\rho_{\alpha h}(\phi)\Omega, \mathbf{v}_h) \tag{91}$$

has $\{\lambda_j\}_{j=1}^{m^*}$ eigenvalues, $\lambda_{j+1} > \lambda_j$, and a corresponding eigenfunction set $\{\Omega_j\}_{j=1}^{m^*}$ satisfying the orthonormal relation

$$(\Omega_i, \Omega_j)_{\rho_h(\phi)} = \int_D \rho_{\alpha h}(\phi)\Omega_i \cdot \Omega_j \, \mathrm{d}x = \begin{cases} 1 & \text{if } i = j \\ 0 & \text{if } i \neq j \end{cases} \tag{92}$$

Since $\rho_\alpha(\phi) > 0$, (92) defines an equivalent $L^2$-inner product in $\mathbf{V}_{h0}$. By virtue of the spectral theory of compact operators it follows that the set $\{\Omega_j\}_{j=1}^{m^*}$ forms an orthonormal basis in $\mathbf{V}_{h0}$ with respect to the inner product $(\cdot,\cdot)_{\rho_\alpha(\phi)}$. Hence, any $\mathbf{v}_h \in \mathbf{V}_{h0}$ can be expressed as

$$\mathbf{v}_h = \sum_{j=1}^{m*} (\mathbf{v}_h, \Omega_j)_{\rho_{\alpha h}(\phi)} \Omega_j$$

and it is easy to see that the following relations hold:

$$A_h \mathbf{v}_h = \sum_{j=1}^{m*} \lambda_j (\mathbf{v}_h, \Omega_j)_{\rho_{\alpha h}(\phi)} \rho_{\alpha h}(\phi) \Omega_j$$

$$(\mathbf{v}_h, \mathbf{u}_h)_{\rho_{\alpha h}(\phi)} = \sum_{j=1}^{m*} (\mathbf{v}_h, \Omega_j)_{\rho_{\alpha h}(\phi)} (\mathbf{u}_h, \Omega_j)_{\rho_{\alpha h}(\phi)}$$

and

$$(A_h \mathbf{v}_h, \mathbf{u}_h) = \sum_{j=1}^{m*} \lambda_j (\mathbf{v}_h, \Omega_j)_{\rho_{\alpha h}(\phi)} (\mathbf{u}_h, \Omega_j)_{\rho_{\alpha h}(\phi)}$$

With this in mind, if we multiply (90) by $\mathbf{u}_h^{n+1}$ we obtain that

$$\sum_{j=1}^{m*} (\mathbf{u}_h^{n+1}, \Omega_j)^2_{\rho_{\alpha h}(\phi_h^{n+1})} = \sum_{j=1}^{m*} \frac{1-\dfrac{\Delta t}{2}\lambda_j}{1+\dfrac{\Delta t}{2}\lambda_j} (\bar{\mathbf{u}}_h^n, \Omega_j)_{\rho_{\alpha h}(\bar{\phi}_h^n)} (\mathbf{u}_h^{n+1}, \Omega_j)_{\rho_{\alpha h}(\phi_h^{n+1})}$$

$$-\sum_{j=1}^{m*} \frac{\Delta t}{1+\dfrac{\Delta t}{2}\lambda_j} (g z_h \nabla \log \rho_{\alpha h}(\phi_h^{n+1}), \Omega_j)_{\rho_{\alpha h}(\phi_h^{n+1})} (\mathbf{u}_h^{n+1}, \Omega_j)_{\rho_{\alpha h}(\phi_h^{n+1})}$$

Let $\Lambda = \operatorname{diag}(\lambda_1, \ldots, \lambda_{m*})$, then $1 - \frac{\Delta t}{2}\lambda_j / 1 + \frac{\Delta t}{2}\lambda_j$ is the $j$th element of the diagonal matrix $(I - \frac{\Delta t}{2}\Lambda)(I + \frac{\Delta t}{2}\Lambda)^{-1}$ whose Euclidean norm is $<1$. Similarly, $1/1 + \frac{\Delta t}{2}\lambda_j$ is the $j$th element of the diagonal matrix $(I + \frac{\Delta t}{2}\Lambda)^{-1}$ whose Euclidean norm is also $<1$. So that, applying Cauchy–Schwarz inequality it follows that

$$\|\sqrt{\rho_{\alpha h}(\phi_h^{n+1})}\mathbf{u}_h^{n+1}\|^2 \leqslant \|\sqrt{\rho_{\alpha h}(\bar{\phi}_h^n)}\bar{\mathbf{u}}_h^n\| \, \|\sqrt{\rho_{\alpha h}(\phi_h^{n+1})}\mathbf{u}_h^{n+1}\|$$

$$+ C\Delta t \|\sqrt{\rho_{\alpha h}(\phi_h^{n+1})} g z_h \nabla \log \rho_{\alpha h}(\phi_h^{n+1})\| \, \|\sqrt{\rho_{\alpha h}(\phi_h^{n+1})}\mathbf{u}_h^{n+1}\|$$

Making use of (85) and (86) we obtain the result. □

A further comment on the expression $\nabla \log \rho_{\alpha h}(\phi_h^{n+1})$ when $\alpha \to 0$ is in order. Noting that

$$\rho_{\alpha h}(\phi_h^{n+1}) = \sum_{i=1}^{\mathrm{MV}} (\rho_\alpha(\phi_h^{n+1}))_i \chi_i$$

it follows that

$$\nabla \log \rho_{\alpha h}(\phi_h^{n+1}) = \frac{1}{\rho_{\alpha h}(\phi_h^{n+1})} \sum_{i=1}^{\mathrm{MV}} (\rho_\alpha(\phi_h^{n+1}))_i \nabla \chi_i$$

By virtue of (19) and (20) and the fact that as $\alpha \to 0$

$$H_\alpha(\phi_h^{n+1}) \to \begin{cases} 0 & \text{if } \phi_h^{n+1} < -\alpha \\ (0,1) & \text{if } |\phi_h^{n+1}| \leqslant \alpha \\ 1 & \text{if } \phi_h^{n+1} > \alpha \end{cases}$$

for all $n$, we have that as $\alpha \to 0 \rho_{\alpha h}(\phi_h^{n+1})$ is bounded by the inequalities $\rho_2 \leqslant \rho_{\alpha h}(\phi_h^{n+1}) \leqslant \rho_1$; this means that $\nabla \log \rho_{\alpha h}(\phi_h^{n+1})$ remains bounded as $\alpha \to 0$.

## 6. NUMERICAL RESULTS

In this section, we use the semi-Lagrangian level set method to compute the numerical solution to various problems. The idea behind these numerical tests is to ascertain the behaviour of the method as regards the following issues: (i) resolution of sharp discontinuities, (ii) redistancing and conservation of volume, and (iii) accuracy of the numerical solution versus real solution. Our first numerical test is the steady advection of a slotted cylinder whose exact solution is known. Then, we solve two typical hydrodynamic problems and compare our numerical results with those obtained in Reference [32] for the first problem and with experimental results [33] for the second problem.

### *6.1. The steady advection test*

This problem was proposed by Zalesack [34] to test the ability of his multidimensional flux corrected scheme to deal with sharp discontinuities and later [16] used it as a benchmark test for their reinitialization scheme. The problem, defined in a square domain $D=(0,1)\times(0,1)$, consists of finding $\phi(x,t)$ such that

$$\begin{aligned} \frac{\partial\phi}{\partial t} + \mathbf{u}\cdot\nabla\phi = 0 \quad \text{in } D\times(0,T] \\ \phi|_{\partial D} = \text{Periodic} \end{aligned} \tag{93}$$

$$\phi(x,0)=\phi_0(x)\equiv \pm\min_{y\in 0}|x-y| \tag{94}$$

where $O$ is a circle of radius 0.15 centred at $(0.5, 0.75)$ with a slot of depth $=0.25$ and width $=0.05$. (See Figure 5). The components of the steady velocity are

$$\begin{aligned} u_1(x,y) &= 0.5 - y \\ u_2(x,y) &= x - 0.5 \end{aligned} \tag{95}$$

To compare our numerical results with those of Reference [16] we construct an initial mesh by partitioning $D$ into $100\times 100$ uniform squares with $h=0.01$ and then, dividing each square into two triangles by joining the left lower vertex with the right upper one. As in Reference [16], the numerical solution is calculated with a time step $\Delta t = h$; this means that 628 time steps are needed to complete a revolution. Following Reference [16], we measure the error by the magnitude

$$\frac{\int_D H(\phi_{\text{exact})}) - H(\phi_{\text{numerical})})\,\mathrm{d}x}{L} \tag{96}$$

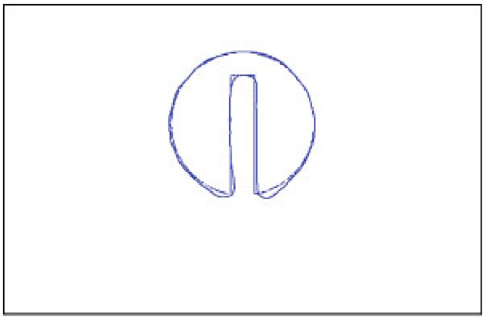

Figure 5. Steady advection test.

where $L$ is the length of perimeter of the slotted circle. Notice that in this numerical test the perimeter of the slotted circle plays the role of an interface. We have performed two runs. The first one uses the parameters $h$ and $\Delta t$ given above, and the second run uses $h_2 = (h/2)$ and $\Delta t_2 = (\Delta t/2)$. We write in Table I the numerical errors (96) obtained in these runs; such results show that (for this example) the order of convergence of the quasi-monotone semi-Lagrangian scheme to compute $\overline{\phi}_h^n(x)$ (see Equations (45)–(56)) plus the reinitialization scheme (see Equations (66)–(75)) is approximately 2 as one would expect. Also, it is worth mentioning that the errors in Table I are smaller than the corresponding ones of Reference [16], where a third-order ENO scheme for space discretization combined with a third-order explicit Runge–Kutta method for time discretization are used for both the advection equation and the reinitialization step to compute the numerical solution $\phi^{n+1}(x)$. We overlay in Figure 5 the numerical solution (full line) obtained in the first run and the exact solution. This figure compares satisfactorily with Figure 5 of Reference [16].

### *6.2. The bottom bump*

We wish to calculate the profile of the wave generated by the flow past a bump located at the bottom of a shallow channel as depicted in Figure 6. The bump is represented by the function

$$y = \frac{27E}{4l^3} x(x-l)^2$$

where $E = 0.042$ m, $l = 0.2$ m and $x$ is the distance from the leading edge. The physical parameters of the problem are $\rho_1 = 998.1\ \mathrm{kg\,m^{-3}}$, $\mu_1 = 10^{-3}\ \mathrm{kg\,m^{-1}\,s^{-1}}$; $\rho_2 = 1.20\ \mathrm{kg\,m^{-3}}$, $\mu_1 = 1.81\times10^{-5}\ \mathrm{kg\,m^{-1}\,s^{-1}}$; $U = 1.985\ \mathrm{m\,s^{-1}}$ and $g = 9.8\ \mathrm{m\,s^{-2}}$. The velocity $(U, 0)$ is the upstream velocity of the flow. Taking $U$ and $l$ as velocity and length scales, respectively, yields as nondimensional control parameters of the flow $Re = 8.74\times10^4$ and $Fr = 2.05$. For this Froude number the flow is super critical. The boundary conditions are the same considered in Figure 1. The mesh is composed of triangles of equal size $h = 0.05$ and the number of nodes MV = 36 584. In the calculations we use a time step $\Delta t = 0.02$. The width of the transition region where free surface is imbedded is $2\alpha = 2h$, and the length of the pseudo time step

Table I.

| $h$ | Error |
|---|---|
| $10^{-2}$ | 1.37E-1 |
| $5\times10^{-3}$ | 3.53E-2 |

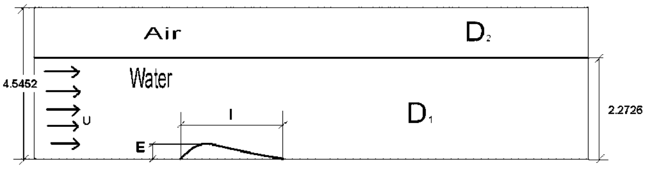

Figure 6. Bottom bump geometry.

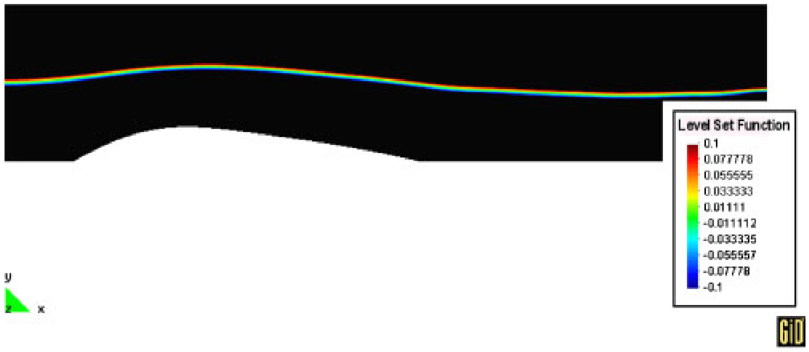

Figure 7. Bottom bump free surface profile at $t = 40$.

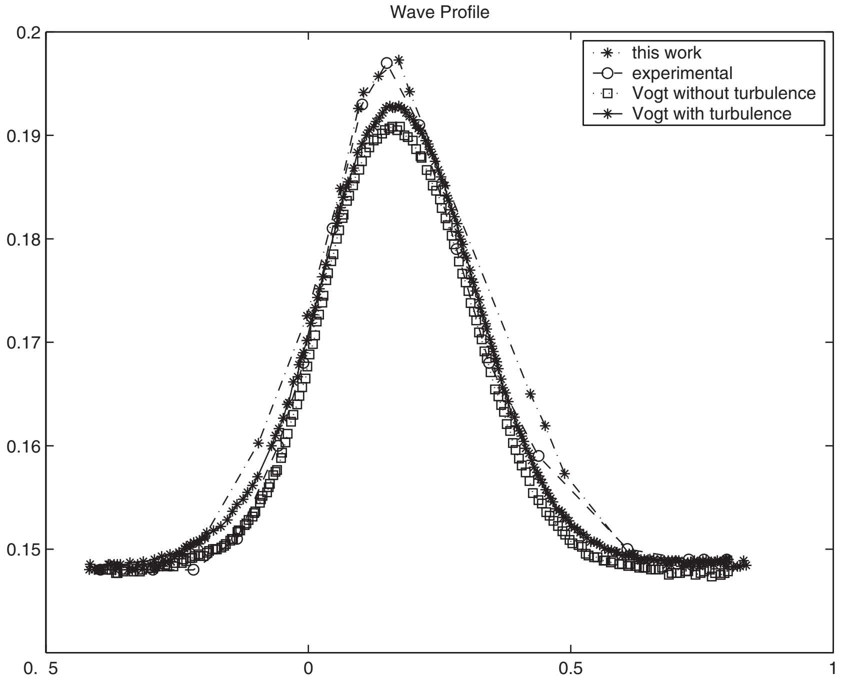

Figure 8. Comparison of free surface profiles at $t = 40$.

in the reinitialization stage is $\Delta\tau = \frac{1}{10}h$. Figure 7 shows the profile of the free surface after 2000 time steps and Figure 8 compares this profile with the experimental profile and the profiles calculated by Vogt [32] with both a $k$–$\varepsilon$ turbulent closure scheme for the Navier–Stokes equations and without turbulent scheme. We should mention that Reference [32] uses a grid of 39 660 nodes and the finite volume technique to formulate the space discretization of the equations. The convective terms of both the Navier–Stokes and the level set equations are calculated either by second-order or third-order or QUICK [35] scheme, whereas the reinitialization stage is performed following the reinitialization formulation of Reference [9] with a second-order ENO scheme. The numerical profile given by our method fits very well the peak of the experimental profile, although it has a slightly wider shape.

### 6.3. *The submerged hydrofoil*

This is a severe test for various reasons. First, a fine grid is needed to resolve the circulation generated at the tip of the foil. Second, in contrast with the bump test where the free surface profile shows a standing elevation located above the bump, now the waves generated travel downstream with the flow, so that they are very sensitive to numerical dispersion and dissipation errors. In order to have an experimental basis to compare with our numerical results, we use a NACA0012 foil as Duncan [33] in his experimental research. The geometry of the problem is shown in Figure 9 where the dimensions are given in non dimensional units. The depth, angle of attack and the chord length of the foil are $s=21\,\text{cm}$, $\beta=5^\circ$ and $l=17.5\,\text{cm}$, respectively.The upstream velocity $(U,0)=(0.8,0)$ in $\text{ms}^{-1}$. Taking $l$ and $U$ as the length and velocity scales of reference, respectively, we have that the Froude and Reynolds numbers of the flow are $Fr=0.567$ and $Re=1.62\times 10^5$. In view of such a high $Re$ number, and given that the purpose of this paper is not to test different turbulent schemes, for simplicity we use in these simulations the so-called Smagorinski turbulence model, which considers that the viscosity coefficient is a function of the modulus of the gradient of the velocity. Specifically, the formulation of the viscous terms of the Navier–Stokes equations in the Smagorinski turbulent model is

$$\nabla\cdot(v_T\nabla\mathbf{u})$$
$$v_T=\rho(\phi)(v(\phi)+C\bar{h}^2|\nabla\mathbf{u}+\nabla\mathbf{u}^{\mathrm{T}}|)$$

where we will assume the simplification of considering $C=0.01$ as a constant parameter, $\bar{h}$ is the average mesh size around the point $x$. Although we know that $C$ is not a constant parameter, and that it is a function of the Reynolds number where its value varies from flow to flow also locally in a flow, see References [36, 37], the value used for $C$ is a typical value used in a RANS context whenever you include turbulent effects using a common simplification of the Smagorinski model. Other authors that make the same considerations in our context are García and Oñate [38] and Ed Akin *et al.* [39]. We take $\bar{h}^2$ as the measure of the element where $x$ is located. Note that a fully implicit time discretization of the viscous terms yields a non linear system of equations to be solved every time step. However, because of limited computational resources, our approach for this example consists of implementing a semi-implicit time discretization of the viscous terms by taking $v_T^n$ in the equation for $\mathbf{u}^{n+1}$.

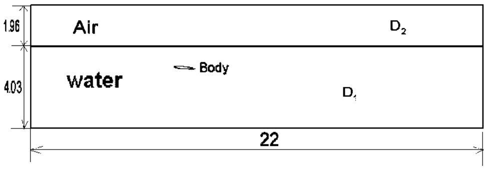

Figure 9. Hydrofoil geometry.

So that, the Stokes problem (60) is now of the form

$$\int_D \rho_{\alpha h}(\phi_h^{n+1})\mathbf{u}_h^{n+1}\cdot\mathbf{v}_h\,\mathrm{d}x + \frac{\Delta t}{2}\int_D \nu_{hT}^n\nabla\mathbf{u}_h^{n+1}\cdot\nabla\mathbf{v}_h\,\mathrm{d}x - \Delta t\int p_h^{n+1}\nabla\cdot\mathbf{v}_h\,\mathrm{d}x = (\mathbf{G}_h^{n+1},\mathbf{v}_h)$$

$$\int_D q_h\nabla\cdot\mathbf{u}_h^{n+1}\,\mathrm{d}x = 0$$

where

$$(\mathbf{G}_h^{n+1},\mathbf{v}_h) = \int_D \rho_{\alpha h}(\phi_h^{n+1})\bar{\mathbf{u}}_h^n\cdot\mathbf{v}_h\,\mathrm{d}x - \frac{\Delta t}{2}\int_D \nu_{hT}^n\nabla\bar{\mathbf{u}}_h^n\cdot\nabla\mathbf{v}_h\,\mathrm{d}x$$
$$-\Delta t\int_D g(\rho_\alpha(\phi_h^{n+1})z)_h\nabla\cdot\mathbf{v}_h\,\mathrm{d}x - \Delta t\int_D gz_h\nabla\rho_{\alpha h}(\phi_h^{n+1})\cdot\mathbf{v}_h\,\mathrm{d}x$$

and

$$\nu_{hT}^n = \rho_{\alpha h}(\phi^{n+1})(\nu_{\alpha h}(\phi^{n+1}) + C\bar{h}^2|\nabla\mathbf{u}_h^n + (\nabla\mathbf{u}_h^{\mathrm{T}})^n|)$$

The boundary conditions are (3)–(6) with the boundary condition (5) on the top boundary. We have run this example with two meshes. The first mesh, see Figure 10 for a detail of the mesh in a neighbourhood around the foil, consists of 38 334 $P_2/P_1$ elements for velocity and pressure and 153 336 $P_1$ elements for the level set function $\phi$ with a total number of nodes $\mathrm{MV} = 77\,432$. As we see in Figure 10, the smallest elements with $h = 0.01$ are located in a small neighbourhood around the foil, then the mesh is progressively coarsening up to reach a size diameter $h = 0.1$ that is kept constant throughout the rest of the mesh. The time step for the computations on this and the finer mesh is $\Delta t = 0.01$. We show in Figure 12

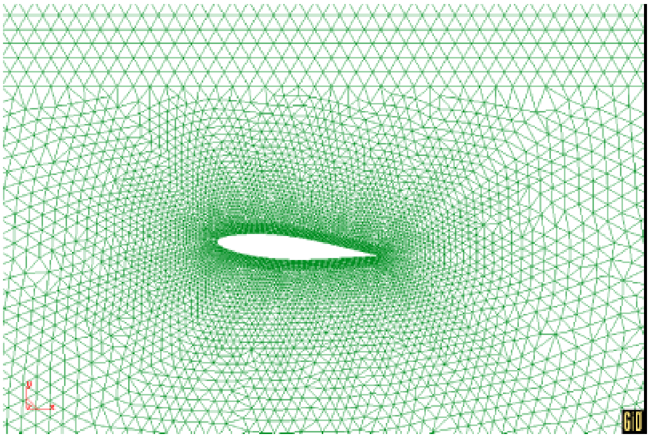

Figure 10. Detail of the mesh around the hydrofoil.

the numerical travelling wave and the travelling wave observed in channel experiments [33] generated by the presence of the hydrofoil in the flow at time $t = 27$ (i.e. after 2700 time steps of integration). It is clear that the numerical wave is shifted with respect to the experimental one, although the period and amplitude of the numerical wave are in good agreement with the experimental ones. A significant improvement of the numerical results is achieved with a refined mesh of 124 748 nodes as we can see in Figure 13, where the numerical solution matches very well the experimental one (Figures 11–13).

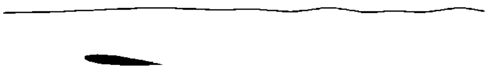

Figure 11. Hydrofoil wave profile at time step $t = 27$.

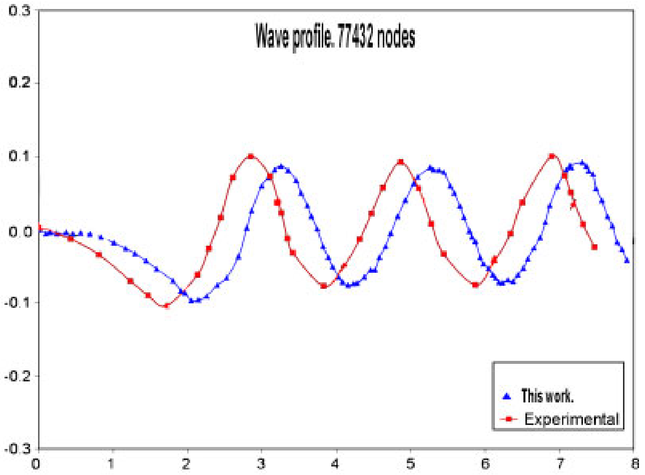

Figure 12. Wave profiles created by the hydrofoil at $t = 27$.

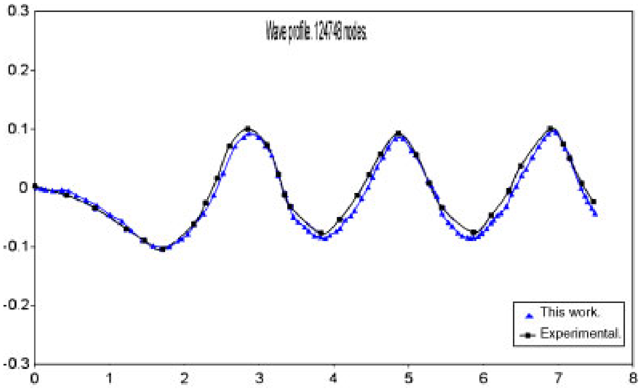

Figure 13. Wave profiles created by the hydrofoil with a finer mesh at $t = 27$.

As general comments on the numerical experiments we say that the Stokes problem is solved by the version of the Uzawa-preconditioned conjugate gradient algorithm presented in Reference [30] with a tolerance for the stopping criterium of $5.0 \times 10^{-5}$. The finite element discretization of the Stokes problem yields a set of symmetric linear systems of equations for the velocity and for the pressure, such systems are solved by ICCG with a tolerance for the stopping criterium of $10^{-5}$. The stopping criterium for the functional iteration in the calculation of the feet of the characteristics is $10^{-3}$.

The calculations presented in the paper were carried out on a standard PC with one processor of 518 Mb of RAM and AMD XP2000 1666 MHz. The average CPU time per time step in the hydrofoil example on the fine mesh is about 36 s.

## ACKNOWLEDGEMENTS

A part of this work was conducted in Laboratorio de Hidrodinámica Marina de la Escuela Técnica Superior de Ingenieros Navales de la Universidad Politécnica de Madrid. So we like to acknowledge the technical, computational and friendly support giving to us by the director and staff of this centre. Dr R. Bermejo was supported by Grants CLI98-1076 and REN2002-03726 from Comisión Interministerial de Ciencia y Tecnología de España and Ministerio de Ciencia y Tecnología de España, respectively.

## REFERENCES

1. Osher S, Sethian JA. Fronts propagating with curvature dependent speed: algorithms based on Hamilton–Jacobi formulations. *Journal of Computational Physics* 1988; 12–49.
2. Sethian JA. *Level Set Methods and Fast Marching Methods*. Cambridge University Press: Cambridge, U.K., 1999.
3. Osher S, Fedkiw R. *Level Set Methods and Dynamic Implicit Surfaces*. Springer: New York, 2003.
4. Harlow FW, Welch JE. Numerical calculation of time dependent viscous incompressible flow. *Physics of Fluids* 1965; **8**:2182–2189.
5. Patel VC, Stern F (eds). *Sixth International Conference on Numerical Ship Hydrodynamics*. Iowa, Naval Studies Board of the U.S.A., National Research Council, IIHR, DTRC and ONR, 1993.
6. Sussman M, Dommermuth D. The numerical simulation of ship waves using Cartesian grid methods. *Twenty-third Symposium of Naval Hydrodynamics* 2001; 762–779.
7. Cura A, Schumann C. Free surface viscous flow around ship models. In *Proceedings of the Seventh International Conference on Numerical Ship Hydrodynamics*, Piquet J (ed.), Nantes, 1999; 1–12.
8. Temperton C, Staniforth A. An efficient two-time level semi-Lagrangian semi-implicit integration scheme. *Quarterly Journal of the Royal Meteorological Society* 1987; **113**:1025–1039.
9. Sussman M, Smereka P, Osher S. A level set approach for computing solutions to incompressible two-phase flow. *Journal of Computational Physics* 1994; **114**:146–159.
10. Strain J. Semi-Lagrangian methods for level set equations. *Journal of Computational Physics* 1999; **151**:498–533.
11. Strain J. A fast modular semi-Lagrangian method for moving interfaces. *Journal of Computational Physics* 2000; **161**:512–536.
12. Allievi A, Bermejo R. Finite element modified method of characteristics for Navier–Stokes equations. *International Journal for Numerical Methods in Fluids* 2000; **32**:439–464.
13. Bermejo R. Analysis of a class of quasi-monotone and conservative semi-Lagrangian advection schemes. *Numerische Mathematik* 2001; **87**:597–623.
14. Bermejo R, Staniforth A. The conversion of semi-Lagrangian advection schemes to quasi-monotone schemes. *Monthly Weather Review* 1992; **120**:2622–2632.
15. Ciarlet PG. *The Finite Element Method for Elliptic Problems*. North-Holland: Amsterdam, 1978.
16. Sussman M, Fatemi E. An efficient, interface-preserving level set redistancing algorithm and its applications to interfacial incompressible fluid flow. *SIAM Journal on Scientific Computing* 1999; **20**:1165–1191.
17. Sussman M, Fatemi E, Smereka P, Osher S. An improved level set method for incompressible two-phase flows. *Computers and Fluids* 1998; **27**:663–689.
18. Barth TJ, Sethian JA. Numerical schemes for the Hamilton–Jacobi and level set equations on triangulated domains. *Journal of Computational Physics* 1998; **145**:1–40.

19. Chessa J, Belytschko T. An extended finite-element method for two phase fluids. *Journal of Applied Mechanics* 2003; **70**:10–17.
20. Quecedo M, Pastor M. Application of the level set method to the finite element solution of two phase flows. *International Journal for Numerical Methods in Engineering* 2001; **50**:645–663.
21. Zienkiewicz O, Codina R. A general algorithm for compressible and incompressible flow. *International Journal for Numerical Methods in Fluids* 1995; **20**(8/9):869–885.
22. Smolarkiewicz PK, Pudykiewicz J. A class of semi-Lagrangian approximations for fluids. *Journal of the Atmospheric Sciences* 1992; **49**:2082–2096.
23. Staniforth A, Coté J. Semi-Lagrangian schemes for atmospheric models a review. *Monthly Weather Review* 1991; **119**:2206–2223.
24. Brenner S, Scott R. *The Mathematical Theory of Finite Elements*. Springer: New York, 1994.
25. Hughes TJR. *The Finite Element Method*. Prentice-Hall: Englewood Cliffs, NJ, 1987.
26. Johnson C. *Numerical Solution of Partial Differential Equations by the Finite Element Method*. Cambridge University Press: Cambridge, U.K., 1987.
27. Brezzi F, Fortin M. *Mixed and Hybrid Finite Element Methods*. Springer: New York, 1991.
28. Girault V, Raviart P-A. *Finite Element Methods for Navier–Stokes Equations*, *Theory and Algorithms*. Springer: Berlin, 1986.
29. Allievi A, Bermejo R. A generalized particle search–locate algorithm for arbitrary grids. *Journal of Computational Physics* 1997; **132**:157–166.
30. Dean EJ, Glowinski R. On some finite element methods for the numerical simulation of incompressible viscous flow. In *Incompressible Computational Fluid Mechanics*, Gunzburger MD, Nicolaides RA (eds). Cambridge University Press: Cambridge, U.K., 1993; 17–66.
31. Showalter R. *Hilbert Spaces Methods for Partial Differential Equations*, 1977.
32. Vogt M. A numerical investigation of the level set method for computing free surface waves. *Technical Report CHA/NAV/R-98/0054*, Department of Naval Architecture and Ocean Engineering, Division of Hydromechanics, Chalmers University of Technology, Goteborg, Sweden, 1998.
33. Duncan JH. The breaking and non breaking wave resistance of a two dimensional hydrofoil. *Journal of Fluid Mechanics* 1983; **33**:303–319.
34. Zalesack S. Fully multidimensional flux-corrected transport algorithms for fluids. *Journal of Computational Physics* 1979; **31**:335–362.
35. Leonard BP. A stable and accurate convective modeling based on quadratic upstream interpolation. *Computer Methods in Applied Mechanics and Engineering* 1979; **19**:59–97.
36. Wilcox DC. *Turbulence Modelling for CFD*. DCW Industries: La Cañada, CA, 1993.
37. Ferziger JH, Peric M. *Computational Methods for Fluid Dynamics* (3rd edn). Springer: Berlin, 2002.
38. García J, Oñate E. An unstructured finite element solver for ship hydrodynamics problems. *Journal of Applied Mechanics* 2003; **70**(1):18–26
39. Ed Akin J, Tayfun T, Mehmet U, Sanjay M. Stabilized formulations and Smagorinsky turbulence model for incompressible flows. In *Fifth World Congress on Computational Mechanics*, Mang HA, Rammerstorfer FG, Eberhardsteiner J (eds), Vienna, Austria, 7–12 July 2002.